

1  
2  
3  
4  
5 Identification of a Lipid Scrambling Domain in ANO6/TMEM16F  
6  
7  
8  
9

10 Kuai Yu <sup>\*</sup>, Jarred M. Whitlock <sup>\*</sup>, Kyleen Lee, Eric A. Ortlund<sup>1</sup>, Yuan Yuan Cui, and H. Criss Hartzell  
11

12  
13 \* Co-first authors contributed equally to this work.  
14  
15  
16  
17  
18

19 Department of Cell Biology and <sup>1</sup>Department of Biochemistry  
20 Emory University School of Medicine  
21 Atlanta, GA 30322  
22  
23

24 **Competing Interests**

25 The authors have no competing financial or non-financial interests.  
26

## Abstract

Phospholipid scrambling (PLS) is a ubiquitous cellular mechanism involving the regulated bidirectional transport of phospholipids down their concentration gradient between membrane leaflets. ANO6/TMEM16F has been shown to be essential for  $\text{Ca}^{2+}$ -dependent PLS, but controversy surrounds whether ANO6 is a phospholipid scramblase or an ion channel like other ANO/TMEM16 family members. Combining patch clamp recording with measurement of PLS, we show that ANO6 elicits robust  $\text{Ca}^{2+}$ -dependent PLS coinciding with ionic currents that are explained by ionic leak during phospholipid translocation. By analyzing ANO1-ANO6 chimeric proteins, we identify a domain in ANO6 necessary for PLS and sufficient to confer this function on ANO1, which normally does not scramble. Homology modeling shows that the scramblase domain forms an unusual hydrophilic cleft that faces the lipid bilayer and may function to facilitate translocation of phospholipid between membrane leaflets. These findings provide a mechanistic framework for understanding PLS and how ANO6 functions in this process.

## Introduction

The transbilayer asymmetric distribution of phospholipids in cell membranes is evolutionarily conserved and essential to cellular physiology. In eukaryotic plasma membranes, the outer leaflet is enriched in phosphatidylcholine (**PtdCho**) and sphingomyelin (**SM**) and the inner cytoplasmic-facing leaflet is rich in phosphatidylserine (**PtdSer**) and phosphatidylethanolamine (**PtdEtn**) (Bretscher, 1972; Fadeel and Xue, 2009; Lhermusier et al., 2011; van Meer, 2011). This asymmetry is established by ATP-dependent lipid flippases, most notably members of the P4 ATPase family (Panatola et al., 2015) and ABC transporters (Borst et al., 2000), that actively transport phospholipids to one leaflet of the membrane and are important in membrane biogenesis. Phospholipid asymmetry plays critical roles in membrane function in two ways. (1) Charges on the phospholipid head groups bind and regulate protein function. The best known examples may be the effects of phosphatidylinositol bispophosphate (PtdInsP<sub>2</sub>) on ion channel proteins (Suh and Hille, 2008), but PtdSer and PtdEtn play equally important roles (Fairn et al., 2011; Hosseini et al., 2014; Jeong and Conboy, 2011; Kay and Grinstein, 2013). (2) The different molecular shapes (e.g.; cylindrical or conical) of various lipids determine membrane curvature which is key to membrane trafficking and fusion (Bigay and Antonny, 2012; Graham and Kozlov, 2010; Suetsugu et al., 2014; Xu et al., 2013).

In opposition to ATP-dependent flippases, ATP-independent phospholipid scramblases (PLSases) facilitate the equilibration of phospholipid distribution between the two membrane leaflets. PLSases play essential roles in the synthesis of glycoconjugates, such as N-glycosylated proteins and GPI-anchored proteins in the endoplasmic reticulum (Pomorski and Menon, 2006). Moreover, at the plasma membrane dissipation of phospholipid asymmetry by phospholipid scrambling (PLS) is a common cell signaling mechanism (Bever and Williamson, 2010; Fadeel and Xue, 2009). For example, exposure of PtdSer on the external leaflet of the plasma membrane marks apoptotic cells for phagocytosis by macrophages and plays a key role in blood clotting (Emoto et al., 1997; Fadok et al., 2001; Fadok et al., 1992; Kay and Grinstein, 2013; Lhermusier et al., 2011; Suzuki et al., 2010; Verhoven et al., 1995). PtdSer exposure that occurs when platelets sense tissue damage serves as a catalytic surface for assembly of plasma-borne coagulation factors and a  $>10^6$ -fold increase in the rate of thrombin formation (Kay et al., 2012; Sahu et al., 2007; Zwaal et al., 1998). PtdSer exposure also plays important roles in developmental processes that involve fusion of mononucleated progenitor cells to form multinucleated cells such as skeletal muscle

(Hochreiter-Hufford et al., 2013; Jeong and Conboy, 2011), osteoclasts (Harre et al., 2012; Helming and Gordon, 2009; Pajcini et al., 2008; Shin et al., 2014; Verma et al., 2014) and placental syncytiotrophoblasts (Huppertz et al., 2006; Riddell et al., 2013).

In the simplest conceptualization, PLS is mediated by phospholipid scramblases (PLSase) that are thought to provide, in a manner analogous to ion channels, an aqueous pathway for the hydrophilic phospholipid head groups to flip between the inner and outer leaflets (Pomorski and Menon, 2006; Sanyal and Menon, 2009). However, the molecular mechanisms of PLS have remained elusive partly because PLS can be catalyzed by a variety of unrelated proteins. PLS is stimulated by two pathways, a rapid one triggered by increases in intracellular  $[Ca^{2+}]$  and a slow caspase-dependent pathway associated with apoptosis (Schoenwaelder et al., 2009). At least four different families of proteins have been implicated in PLS (Bever and Williamson, 2010; Lhermusier et al., 2011; Sahu et al., 2007). The first putative phospholipid scramblases (PLSCR1 – PLSCR4) were identified by their ability to stimulate  $Ca^{2+}$ -dependent PtdSer scrambling when incorporated into liposomes (Basse et al., 1996; Comfurius et al., 1996), but the role of PLSCRs in PLS is controversial because these proteins are small calmodulin-like molecules whose disruption in mice, flies, and worms has little effect on PLS (Acharya et al., 2006; Bever and Williamson, 2010; Fadeel and Xue, 2009; Ory et al., 2013). More recently, the Xk-family protein Xkr8 has been shown to be necessary for caspase-dependent PtdSer scrambling that can be rescued by multiple Xkr8 paralogs (Suzuki et al., 2013a; Suzuki et al., 2014). Unexpectedly, several G-protein coupled receptors including rhodopsin and the  $\beta$ -adrenergic receptor have also been shown to elicit PLS (Goren et al., 2014). Although lipid-translocating ABC transporters and phospholipid synthesis may also play roles in PLS, these processes cannot fully explain PLS (Fadeel and Xue, 2009; Goren et al., 2014).

Recently, it has been suggested that some members of the 10-gene Anoctamin (TMEM16) family are PLSases. Evidence supporting a role for ANO6 in PLS includes the findings that (a) mutations in ANO6 produce Scott Syndrome, a blood clotting disorder where platelets fail to expose PtdSer in response to cytosolic  $Ca^{2+}$  increases (Kmit et al., 2013; Suzuki et al., 2010; Yang et al., 2012), (b) knockout of ANO6 in mice abolishes the ability of cells to expose PtdSer and to scramble other lipid species in response to elevated cytosolic  $Ca^{2+}$  while PLS stimulated by the apoptotic Fas receptor is unaffected (Suzuki et al., 2010), and (c) over-expression of ANO6 in knockout cells rescues PLS (Suzuki et al., 2013b). However, the suggestion that ANO6 is a PLSase is confounded by the fact that other members of the anoctamin family, ANO1 and ANO2, encode the pore-forming subunits of  $Ca^{2+}$ -activated  $Cl^-$  channels (CaCCs) (Caputo et al., 2008; Duran and Hartzell, 2011; Hartzell et al., 2009; Pedemonte and Galletta, 2014; Ruppertsburg and Hartzell, 2014; Schroeder et al., 2008; Yang et al., 2008). It was initially presumed that all ANOs are  $Cl^-$  channels because of the close sequence similarity between ANO family members (ANO1 is 38 - 45% identical to ANOs -3 to -7, >90% coverage), however, the requirement of ANO6 for  $Ca^{2+}$ -dependent PLS and the ability of ANOs 3, 4, 6, 7, and 9 to rescue this activity suggests functional divergence within the ANO family (Suzuki et al., 2013b; Suzuki et al., 2010).

Questions remain whether ANO6 is a PLSase itself and/or is an ion channel that regulates PLSase activity (Kunzelmann et al., 2014; Pedemonte and Galletta, 2014; Picollo et al., 2015). ANO6 has been reported to be a non-selective cation channel (Adomaviciene et al., 2013; Yang et al., 2011), a swelling-activated  $Cl^-$  channel (Almaca et al., 2009), an outwardly-rectifying  $Cl^-$  channel (Martins et al., 2011), a CaCC (Juul et al., 2014; Shimizu et al., 2013; Szteyn et al., 2012), and a CaCC of delayed activation

111 (Grubb et al., 2013). Furthermore, in contrast to Suzuki et al. (Suzuki et al., 2010), Yang et al (Yang et al.,  
112 2012) conclude that ANO6 is a regulator of an endogenous PLSase because they find that expression of  
113 ANO6 in HEK cells does not cause PtdSer exposure. However, the suggestion that some ANOs are  
114 PLSases and are not simply regulators of endogenous PLSases is supported by recent reports that two  
115 fungal ANO homologs purified and incorporated into liposomes mediate  $\text{Ca}^{2+}$ -stimulated PLS (Brunner et  
116 al., 2014; Malvezzi et al., 2013).

117 Here we address three questions. (1) Does expression of ANO6 stimulate  $\text{Ca}^{2+}$ -dependent PLS in  
118 HEK cells? We find that ANO6 expression in HEK cells induces robust  $\text{Ca}^{2+}$ -activated scramblase  
119 activity. (2) Is the ion channel activity of ANO6 related to PLS? We find that ANO6 currents are non-  
120 selective among ions and are activated simultaneously with PLS. This suggests that ionic currents are a  
121 consequence of phospholipid translocation. Chimeric constructs that exhibit PLS also exhibit  
122 simultaneous non-selective currents. Furthermore, we find that drugs that block ANO1 currents do not  
123 block ANO6 currents or PLS. This is consistent with the idea that the ion conduction pathway associated  
124 with ANO6 is unlike the ANO1 pore. (3) What are the domains of ANO6 that are required for  
125 phospholipid scrambling? We find that mutating several amino acids in ANO6 between TMD4 and  
126 TMD5 eliminates both phospholipid scrambling and ion channel activity. Furthermore, replacing as few  
127 as 15 amino acids in ANO1 in the TMD4-TMD5 region with ANO6 sequence confers robust PLS activity  
128 on ANO1, which normally does not elicit PLS activity.

129

130

## Results

131

132 *ANO6 expression induces robust phospholipid scrambling in HEK cells.* We first asked whether  
133 ANO6 when expressed heterologously induced PLS in HEK293 cells.  $\text{Ca}^{2+}$ -dependent PtdSer exposure on  
134 the outer leaflet of the plasma membrane was measured by confocal imaging of two PtdSer probes, either  
135 LactoglobulinC2 fused to Clover fluorescent protein (“LactC2”) or Annexin-V conjugated to AlexaFluor-  
136 568 (“Annexin-V”) (Hou et al., 2011; Kay and Grinstein, 2011; Shi et al., 2006). Our initial experiments  
137 employed LactC2 with a clonal cell line stably transfected with mANO6-FLAG<sub>3X</sub>. 100% of the cells  
138 express ANO6-FLAG<sub>3X</sub> as shown by staining with anti-FLAG antibody (Figure 1A). Intracellular  $\text{Ca}^{2+}$   
139 was elevated by incubation of the cells in 10  $\mu\text{M}$  A23187 in nominally zero  $\text{Ca}^{2+}$  solution followed by  
140 washout of A23187 and addition of 5 mM  $\text{Ca}^{2+}$  to initiate  $\text{Ca}^{2+}$ -dependent PLS. Twelve minutes after  
141 adding  $\text{Ca}^{2+}$ , ~92% of the cells (N = 404) showed LactC2 binding to the surface (Figure 1B,G). In  
142 contrast, little or no LactC2 binding was seen in the parental cell line (0.2% positive cells, N = 724) or in  
143 ANO1-FLAG<sub>3X</sub>-expressing cells (8% positive cells, N = 316) (Figure 1C,D,G). The difference in PLS  
144 observed with ANO1 and ANO6 expressing cells was not explained by differences in expression as  
145 shown by western blot (Figure 1F). These data show clearly that ANO6 expression facilitates PLS.  
146 However, the finding that a small fraction (8%) of ANO6-FLAG<sub>3X</sub> expressing cells do not exhibit PLS  
147 raises the possibility that ANO6 may not be sufficient for PLS and may require additional components.

148 An advantage of LactC2 is that it does not require  $\text{Ca}^{2+}$  to bind PtdSer (Kay and Grinstein, 2011;  
149 Shi et al., 2006), so we were able to use it to test whether ANO6-elicited PtdSer exposure requires  $\text{Ca}^{2+}$ .  
150 ANO6-FLAG<sub>3X</sub> cells exposed to A23187 without addition of  $\text{Ca}^{2+}$  exhibited no detectable LactC2 binding  
151 over 15 min, whereas subsequent addition of  $\text{Ca}^{2+}$  stimulated robust LactC2 binding (Figure 1E).

152 Next, we compared LactC2 and Annexin-V as probes for PLS. The percentage of cells stained  
with Annexin-V and LactC2 were the same, however, the kinetics of binding of the two probes were

markedly different. After elevating cytosolic  $\text{Ca}^{2+}$ , Annexin-V fluorescence increased mono-exponentially with a mean  $\tau = 143$  sec (7 separate experiments,  $\chi^2$  of fit = 0.03) and approached a plateau within less than 10 min (Figure 1H). In contrast, the time course of LactC2 binding was significantly slower (5 separate experiments,  $\tau = 433$  sec,  $\chi^2$  of fit = 0.02). LactC2 binding exhibited a lag period of 1 – 2 min before binding was detectable. One potential explanation of the difference in Annexin-V and LactC2 time courses may be related to the fact that LactC2 prefers binding to oxidized PtdSer (Tyurin et al., 2008). Because Annexin-V binds with more rapid kinetics, the rest of the experiments shown here were performed using Annexin-V.

Because all of the cells in the clonal cell line express ANO6-FLAG<sub>3X</sub> at about the same level, we turned to a polyclonal cell line stably expressing ANO6-EGFP to evaluate the relationship of ANO6 expression to the rate and extent of Annexin-V binding (Figure 2). In the polyclonal line, ANO6-EGFP expression level was variable and 85% of ANO6-EGFP cells exhibited PLS (N = 180). This percentage may be lower than the ANO6-FLAG<sub>3X</sub> clonal line because some ANO6-EGFP positive cells may have lower expression than the ANO6-FLAG<sub>3X</sub> cells. There was a direct relationship between the level of ANO6-EGFP expression and the level of Annexin-V binding 10 min after elevating cytosolic  $\text{Ca}^{2+}$  (Pearson correlation coefficient = 0.84) (Figure 2C), however there was considerable variation around the fitted relationship, with some highly-expressing ANO6 cells showing little Annexin-V binding and low-expressing cells showing high levels of binding. The rate of Annexin-V binding was similar among cells ( $\tau$  in this experiment ranged from 152 – 229 sec), but the plateau level of Annexin-V binding attained after 12 min varied markedly among cells. Neither the rate nor the plateau level of binding correlated with the level of ANO6-EGFP fluorescence. This lack of correlation may reflect an inability to distinguish between ANO6-EGFP located on vs. adjacent to the plasma membrane or may reflect heterogeneity in the expression of other components required for PLS.

*ANO6 current activates in parallel with PLS.* The next question that we sought to answer was whether the ionic current that has been associated with ANO6 (Almaca et al., 2009; Grubb et al., 2013; Harper and Poole, 2013; Juul et al., 2014; Martins et al., 2011; Shimizu et al., 2013; Szteyn et al., 2012; Yang et al., 2011) is linked to PLS or is an independent function of the protein. We patch-clamped HEK cells transiently expressing ANO6-EGFP and recorded ANO6 currents while simultaneously imaging Annexin-V binding. A typical experiment is shown in Figure 3A with average results in Figure 3B-C. After establishing whole-cell recording, the time course of activation of membrane currents in ANO6-expressing cells was very slow even when the patch pipet solution contained high (200  $\mu\text{M}$ )  $\text{Ca}^{2+}$ . The currents typically began to increase 8 min after initiating whole cell recording, which is similar to that reported by others (Grubb et al., 2013). Annexin-V binding usually became detectable 2 - 3 min later (Figure 3B-C). The time courses of ANO6 current activation and Annexin-V binding were fit to the equation  $y = A_2 + (A_1 - A_2) / (1 + \exp[(t - t_0) / \tau])$ . Although the time constants of the increases in Annexin-V binding ( $\tau = 2.24 \pm 0.15$  min) and ANO6 current ( $\tau = 2.31 \pm 0.34$  min) were the same, the time ( $t_0$ ) at which Annexin-V fluorescence reached half of its maximal value  $[(A_1 + A_2) / 2]$  was delayed 3 min relative to the current. In contrast to ANO6, ANO1 currents activated quickly after initiating whole-cell recording and then ran down with time (Figure 3B), as previously reported (Yu et al., 2014) and no Annexin-V binding was observed.

There are two explanations for the lag between ANO6 current activation and Annexin-V binding. One possibility is that current is required for PLS. However, we believe that the lag is partly explained by

195 inherent differences in way the two events are measured. Patch clamp recording measures membrane  
196 conductance instantaneously, while detection of Annexin-V fluorescence requires the accumulation of  
197 Annexin-V on the membrane that is limited by its binding kinetics and the sensitivity of the fluorescence  
198 detection. Because Annexin binding to model bilayers is known to be slow and requires a threshold  
199 PtdSer concentration (Kastl et al., 2002; Shi et al., 2006) and the numerical aperture of the microscope  
200 objective was 0.6, we believe that currents and PLS occur contemporaneously. This correlation suggested  
201 the possibility that currents reflect transmembrane ion leakage associated with the process of phospholipid  
202 transport. The alternative hypothesis that ionic current through ANO6 somehow activates PLS is excluded  
203 by the finding that PLS occurs normally in ANO6-expressing cells under conditions where there is no  
204 ionic current (for example, cells voltage-clamped at 0 mV with identical intracellular and extracellular  
205 solutions where  $E_{rev}$  for every ion is 0 mV).

206 *ANO6 current and PLS require the same  $Ca^{2+}$  concentration for activation.* If ANO6 current is a  
207 consequence of PLS and not a separate function of the protein, we would expect that current and PLS  
208 would require the same  $Ca^{2+}$  concentration for activation. Activation of ANO6 current requires  $>20 \mu M$   
209 free  $Ca^{2+}_i$  and requires minutes to develop (Figure 4A,B). With  $20 \mu M Ca^{2+}$ , neither PLS nor currents are  
210 observed even after 20 min of recording. Currents and PLS are consistently observed only with  $200 \mu M$   
211  $Ca^{2+}$ . Although this finding does not exclude the possibility that ion conductance and PLS are separate  
212 functions of ANO6, it is consistent with the two functions being linked.

213 *The ANO6 current is non-selective.* If one accepts the proposal that ANO6 currents and Annexin-  
214 V binding occur simultaneously, this suggests that ANO6 currents may represent the flux of ions through  
215 micro-disruptions of the lipid membrane occurring during PLS rather than ions flowing through a defined  
216 aqueous pore defined by ANO6 protein. If ANO6 currents are a consequence of PLS, we would predict  
217 that their ionic selectivity would be very low. To explore the idea that ANO6 currents are essentially leak  
218 currents, we examined the ionic selectivity of the currents appearing after PLS was activated. In  
219 comparison to ANO1 currents, which exhibit robust anion:cation selectivity ( $P_{Na}/P_{Cl} = 0.03$ ), the ANO6  
220 current is highly non-selective (Figure 5). The ionic selectivity sequence was  $Na^+ > Cl^- > Cs^+ > NMDG^+$   
221 ( $P_{Na}/P_{Cl} = 1.38$ ,  $P_{Cs}/P_{Cl} = 0.6$ ,  $P_{NMDG}/P_{Cl} = 0.48$ ). These data are consistent with the permeation pathway  
222 of ANO6 being relatively large and capable of passing  $NMDG^+$  which has a mean diameter of  $\sim 7.3 \text{ \AA}$ .  
223 The finding that ANO6 currents have very low ionic selectivity and are activated contemporaneously with  
224 PLS over the same  $Ca^{2+}$  concentration range suggested that PLS and currents have the same underlying  
225 mechanism.

226 *Identification of a protein domain required for scrambling.* Because ANO1 has no scramblase  
227 activity while ANO6 does (Brunner et al., 2014; Malvezzi et al., 2013; Suzuki et al., 2013b; Terashima et  
228 al., 2013), we hypothesized that ANO6 contains a domain responsible for PLS that is absent in ANO1.  
229 We employed computational approaches to gain insights into sequence differences that could define this  
230 functional difference. We analyzed Type-I and Type-II divergence between mammalian ANO1 and  
231 ANO6 as an indication of the functional relevance of different amino acids (Gu, 2006). Sequences used  
232 for the analysis are shown in Figure 6-figure supplement 1 and an alignment of ANO6 and ANO1 is  
233 shown in Figure 6-figure supplement 2. Type I divergence occurs shortly after gene duplication and is  
234 characterized by amino acids that are highly conserved in one paralogous group of proteins and highly  
235 divergent in the other. Type II divergence occurs later when specific functions undergo positive selection  
236 within a paralogous group, resulting in conserved changes in amino acid properties. Type II divergence is

exemplified by alignment positions that are identical within paralogous groups but have amino acids with radically different properties between paralogous groups. There are three major regions of Type-II divergence between ANO1 and ANO 6 (Figure 6A). These regions are located in (a) intracellular loop 1, (b) TMD4 and TMD5 and the short intracellular loop between them, and (c) the C-terminus adjacent to the last transmembrane domain. To test the functional significance of these divergent amino acids, we made chimeric constructs of ANO1 and ANO6, named X-Y-X<sub>*i-j*</sub>, where ANO paralog X has its amino acids *i-j* replaced with aligned amino acids from ANO paralog Y. The 1-6-1 chimeras, made by replacing short segments of ANO1 sequence with ANO6 sequence, were first screened by confocal microscopy of cultures.

Of twenty-six 1-6-1 chimeras, seventeen trafficked to the plasma membrane and generated Cl<sup>-</sup> currents in patch clamp (Figure 6B, Figure 6 - figure supplement 3). Thirteen 1-6-1 chimeras did not exhibit PLS. However, 4 chimeras having ANO1 sequence replaced with ANO6 sequence in the region spanning TMD4 and TMD5 showed robust PLS activity (chimeras 1-6-1\_D554-K588, 1-6-1\_C559-F584, 1-6-1\_S532-G558, and 1-6-1\_D554-V569). The 1-6-1 chimera that scrambled having the smallest ANO6 sequence (1-6-1\_D554-V569) had 15 amino acids of ANO1 replaced with amino acids 525-540 from ANO6. Additional constructs were made in which only pairs or triplet amino acids in ANO1 were mutated to the divergent amino acids from ANO6, but none of these chimeras exhibited PLS activity (Figure 6-figure supplement 4). We term this region of ANO6 between amino acids 525 – 559, capable of conferring PLS activity on ANO1, the scrambling domain (SCRD) (Figure 6C).

The ability of the SCRD to confer PLS activity on ANO1 does not necessarily prove that it is required for ANO6 PLS. To test this possibility, we mutated these amino acids in ANO6 to determine if they abolished ANO6-mediated PLS. Chimeras in which portions of the ANO6 SCRD were replaced with ANO1 sequence had greatly reduced PLS activity (Figure 6-figure supplement 5). Furthermore, mutation of several triplets of amino acids (525NTI, 529EKV, and 533IMI) between N525 and I535 abrogated ANO6 PLS activity.

Chimeras that trafficked to the plasma membrane, as judged by confocal microscopy, were then subjected to patch clamp analysis to measure ionic currents generated during PLS. Figure 7A,B shows the percentage of cells that bound Annexin-V after 15 min whole cell patch clamp recording using 200  $\mu$ M Ca<sup>2+</sup> in the patch pipet and the amplitude of the ionic current at +100 mV when Annexin-V binding had plateaued (see also Figure 6-figure supplements 3-5). Chimeras that support PLS invariably had ionic currents, while 6-1-6 chimeras that do not scramble (6-1-6\_N525-Q559, 6-1-6\_N525-I527, 6-1-6\_E529-V531, and 6-1-6\_N541-T662) exhibited very small or no currents. However, the amplitudes of the currents did not correlate with the percentage of cells that exhibited PLS, possibly because of differences in surface expression, which were not controlled (Figure 7A,B). The finding that mutations in ANO6 that abolished PLS also abolish ionic currents suggests that ions and phospholipids are translocated by overlapping molecular machinery.

To investigate the properties of the chimeras in more detail, we selected the PLS-positive chimera 1-6-1\_D554-K588 and the PLS-negative chimera 6-1-6\_N525-I527 for analysis. We first examined PLS in intact cells after elevation of cytosolic Ca<sup>2+</sup> with A23187. Like ANO6, 1-6-1\_D554-K588 exhibited robust Annexin-V binding within 10 min (Figure 7C). In contrast, 6-1-6\_N525-I527, which had 3 amino acids of ANO6 swapped with ANO1 sequence, did not exhibit PLS (Figure 7C). 96% of cells transfected with 1-6-1\_D554-K588 (N = 178) of cells bound Annexin-V (Figure 7D). In contrast, only 15% of the

279 cells (N = 127) transfected with 6-1-6\_N525-I527 bound Annexin-V. The rate of Annexin-V binding was  
280 very similar for 1-6-1\_D554-K588 and ANO6 (Figure 7E). On average, Annexin-V binding to ANO6-  
281 expressing cells occurred with  $\tau = 143$  sec (Figure 2D), whereas Annexin-V binding in cells transfected  
282 with 1-6-1\_D554-K588 occurred with  $\tau = 218$  sec,  $\chi^2 = 0.03$ ). Although other 1-6-1 chimeras that  
283 exhibited PLS were not investigated at the same detail, the characteristics of PLS of these chimeras were  
284 qualitatively similar to 1-6-1\_D554-K588.

285 Patch clamp analysis shows that the currents of chimeras exhibiting PLS have properties that are a  
286 hybrid of ANO1 and ANO6 (Figure 7-figure supplement 1). While no PLS and no currents were observed  
287 in cells transfected with 6-1-6\_N525-I527 during 20 min using 200  $\mu\text{M}$   $\text{Ca}^{2+}_i$ , in cells transfected with 1-  
288 6-1\_D554-K588, robust Annexin-V binding occurred even with 20  $\mu\text{M}$   $\text{Ca}^{2+}_i$ . Therefore, it seems that this  
289 chimera retains the  $\text{Ca}^{2+}$  sensitivity of ANO1. Moreover, the current was largest immediately upon  
290 establishing whole cell recording and then it ran down with time, similar to ANO1 currents (Figure 7-  
291 figure supplement 1). However, the rundown was not monotonic, but was interrupted by a transient  
292 increase in current. We interpret these data to indicate that this chimera initially exhibits ANO1-like  
293 currents, and that as PLS begins, the current acquires the properties of ANO6. The nature of this current is  
294 investigated below.

295 *Ionic currents associated with scrambling.* We reasoned that if the pathway taken by ions is the  
296 same as the one taken by phospholipids, the two events might have similar pharmacology. Therefore, we  
297 tested the effects of MONNA, a small molecule that blocks ANO1 currents (Oh et al., 2013). We find that  
298 although 10  $\mu\text{M}$  MONNA blocks ANO1 currents  $\sim 90\%$ , ANO6 currents are unaffected (Figure 8A).  
299 These data support the suggestion that the permeation pathway for  $\text{Cl}^-$  in ANO1 differs from the ion  
300 conduction pathway of ANO6. Furthermore, MONNA does not block currents of 1-6-1 chimeras that  
301 exhibit PLS activity (Figure 8A). This suggests that the structural determinants of PLS in the SCRD alter  
302 that pharmacology of ANO1.

303 We have previously shown that ANO1 currents can be activated by strong depolarizations in the  
304 absence of  $\text{Ca}^{2+}$  (Xiao et al., 2011). Because ANO6 does not exhibit such  $\text{Ca}^{2+}$ -independent currents, we  
305 asked whether we could detect  $\text{Ca}^{2+}$ -independent ANO1-like currents in 1-6-1\_D554-K588 in zero  $\text{Ca}^{2+}$ .  
306 Like ANO1, 1-6-1\_D554-K588 exhibits  $\text{Ca}^{2+}$ -independent currents at very positive potentials and these  
307 currents are blocked by MONNA (Figure 8B, blue triangles). This current is  $\text{Cl}^-$ -selective ( $P_{\text{Cs}}:P_{\text{Cl}} = 0.08$ )  
308 (Figure 8C). Thus, in zero  $\text{Ca}^{2+}$  1-6-1\_D554-K588 currents resemble ANO1. However, after PLS has  
309 been activated by  $\text{Ca}^{2+}$ , the current is not blocked by MONNA (Figure 8B, red squares) and the current is  
310  $>4$ -fold less  $\text{Cl}^-$ -selective ( $P_{\text{Cs}}:P_{\text{Cl}} = 0.39$ ) (Figure 8D). These data suggest that as PLS develops in  
311 response to elevated intracellular  $\text{Ca}^{2+}$ , the ionic conductance pathway changes from  $\text{Cl}^-$ -selective to non-  
312 selective. In fact, this transition between MONNA-sensitive and MONNA-insensitive currents can be  
313 seen when MONNA is applied shortly after establishing whole-cell recording with  $\text{Ca}^{2+}$  in the pipet  
314 (Figure 8B, black open circles). The current is initially blocked partially by MONNA, but then the current  
315 begins to increase coincidently with development of PLS.

316 Because PLS of 1-6-1\_D554-K588 develops quickly after establishing whole cell recording, it is  
317 difficult to compare the properties of the currents before and after PLS in the same cell. Therefore, we  
318 used the chimera 1-6-1\_S532-G558 which activates PLS more slowly. About 5 min after establishing  
319 whole-cell recording before PLS was detectable, the current exhibited  $\text{Cl}^-$ -selectivity as indicated by a 35  
320 mV shift in  $E_{\text{rev}}$  upon switching from 150 mM CsCl to 15 CsCl ( $P_{\text{Cs}}:P_{\text{Cl}} = 0.15$ ) (Figure 8E). In contrast,



after scrambling had occurred, cation permeability was significantly increased, with an  $\Delta E_{rev}$  shift of only 15 mV ( $P_{Cs}:P_{Cl} = 0.50$ ) (Figure 8F). We cannot formally determine whether the  $Cl^-$ -selective pathway in the absence of PLS and the non-selective PLS-linked pathway are the same, but the observation that MONNA blocks the  $Cl^-$ -selective pathway but has no effect on the current after PLS develops suggests that the  $Cl^-$ -selective pathway is no longer present after PLS occurs. This is consistent with the  $Cl^-$ -selective pathway becoming less selective during scrambling.

**Homology Model of ANO6.** Recently, the X-ray structure of an ANO homolog from the fungus *Nectria haematococca* was published (Brunner et al., 2014). This protein, nhTMEM16, exhibits PLS activity when reconstituted into liposomes. Evidence for its channel activity is lacking, although the authors indicate that the lack of channel activity might be an artifact of the purification and reconstitution conditions. To gain insights into the structure-function relationships of the SCR to protein structure, we created a homology model of ANO6 based on nhTMEM16 (Figure 9). This model shows that the SCR forms a unique structure. Along with helices 3, 6, and 7, it forms what Brunner et al. (Brunner et al., 2014) call the “subunit cavity,” a hydrophilic crevice that faces the lipid membrane on the side of the protein away from the dimer interface. Brunner et al. speculate that this region may be involved in lipid transport.

## Discussion.

**The scrambling pathway of ANO6.** Phospholipid scramblases are conceived to function in a fashion similar to ion channels by forming an aqueous pore for the polar head groups of the phospholipids to cross the hydrophobic center of the membrane (Pomorski and Menon, 2006; Sanyal and Menon, 2009). The recent 3-dimensional structure of nhTMEM16, which catalyzes phospholipid scrambling when incorporated into lipid vesicles, provides key insights into this process (Brunner et al., 2014). The authors noticed a peculiar hydrophilic cavity facing the hydrophobic bilayer that they propose may be involved in lipid scrambling, although no lipids were visualized in the structure. The idea that this cleft may be the phospholipid “channel” is supported by our ANO6 homology model that predicts that the SCR forms one side of this cleft. Intriguingly, residues located in TMD7-TMD8 of ANO1, identified for their roles in  $Ca^{2+}$  binding and gating, make up the other side of this hydrophilic cavity (Bill et al., 2015; Tien et al., 2014; Yu et al., 2012) (Figure 9D,E). The  $Ca^{2+}$  binding site, therefore, is well situated to control structural rearrangements of the hydrophilic cleft to provide a potential pathway for phospholipid translocation.

**Is ANO6 a PLSase?** An important role of ANO6 in PLS seems well established (Suzuki et al., 2013b; Suzuki et al., 2010), although its identity as a PLSase has been contested (Yang et al., 2012). This debate has attracted considerable attention (Harper and Poole, 2013; Kmit et al., 2013; Kunzelmann et al., 2014; Pedemonte and Galletta, 2014). It is important to note that despite the motivation to conclude that ANO6 is a PLSase based on its similarity in structure to nhTMEM16, it remains a possibility that ANO6 is a regulator of another protein that is the PLSase. Our finding that only about 92% of cells expressing ANO6 exhibit PLS suggests that ANO6 is not sufficient for PLS. Further, the lack of correlation between ANO6 expression levels and PLS activity supports some skepticism. One must only recall that PLSCR1 incorporated into liposomes mediates PLS but that knockout of its gene does not have clear-cut effects on PLS to appreciate a need for caution (Acharya et al., 2006; Bevers and Williamson, 2010; Fadeel and Xue, 2009; Ory et al., 2013).

362       *The ion conduction pathway.* We propose that during scrambling ions pass through the same  
363 pathway that is occupied by the phospholipid. Ions might accompany the phospholipids as counterions or  
364 may simply flux independently through the same pathway. This suggestion is based on the observation  
365 that PLS and ionic currents activate contemporaneously and exhibit similar sensitivity to  $\text{Ca}^{2+}$ .  
366 Furthermore, the presence of non-selective, slowly-activating currents that are insensitive to the ANO1  
367 inhibitor MONNA correlate with the ability of chimeras to scramble. Some support for this idea is  
368 provided by cysteine mutagenesis and accessibility experiments showing that amino acids that we believe  
369 form the vestibule of the  $\text{Cl}^-$  selective pore of ANO1 (Yu et al., 2012) are located at the extracellular  
370 surface of the hydrophilic cleft (Figure 9-figure supplement 1).

371       *Evolution of the ANO/TMEM16 family.* Our data add to the already growing awareness that the  
372 ANO family is functionally split with some of its members being anion-selective ion channels (ANO1 and  
373 ANO2) and other members having the ability to transport lipids between membrane leaflets. This  
374 functional duplicity is reminiscent of two other anion channels, CFTR and CLCs, which apparently  
375 evolved from transporters. CFTR (cystic fibrosis transmembrane conductance regulator) is a  $\text{Cl}^-$  channel  
376 that evolved from ABC transporters (Gadsby et al., 2006; Jordan et al., 2008; Miller, 2010), and the CLC  
377 chloride channels CLC-1 and CLC-2 are members of a 9-gene family most of which are  $\text{H}^+$ - $\text{Cl}^-$   
378 exchangers (Lisal and Maduke, 2008; Miller, 2006). Additionally, the P4 ATPases that function as lipid  
379 flippases evolved from a family of ion transporters (Baldridge and Graham, 2013; Lopez-Marques et al.,  
380 2014). One might speculate that the primordial ANO was a lipid transporter. During evolution, functional  
381 divergence likely occurred after gene duplication where the selective pressure for the major function (lipid  
382 transport) decreased, thus enabling the enhancement of the minor sub-function (ion transport). The  
383 finding that fungi have only one ANO gene, but that some fungal ANO homologs have PLS activity  
384 (Brunner et al., 2014; Malvezzi et al., 2013), supports the idea that PLS is an ancient function of ANOs.  
385 Our data suggest that the ionic currents carried by ANO6 are essentially flowing along with the  
386 scrambling lipids. Thus, the non-selective ion transport that occurs concomitantly with PLSase activity  
387 may have been a sub-function in the ancestral ANO. After gene duplication occurred, this sub-function  
388 may have evolved  $\text{Cl}^-$  ion specificity.

389       ANOs that have evolved into anion channels may be more  $\text{Cl}^-$  selective than the scrambling ANOs  
390 simply because the energy contour of the conduction pathway is altered by the absence of lipid substrate.  
391 Because  $\text{Cl}^-$  is more hydrophobic than its cationic cousins, it may be more suited to traverse the  
392 evolutionary remnants of the phospholipid pathway. Consistent with this idea is the fact that, compared to  
393 many voltage-gated cation channels,  $\text{Cl}^-$  channels are sadly non-selective: virtually all anions permeate  
394 and cations are often significantly permeable (Duran et al., 2010). The pores of  $\text{Cl}^-$  channels are often  
395 modeled as large viaducts that provide selectivity based largely on ionic hydration energies (Dawson et  
396 al., 1999; Liu et al., 2003; Qu and Hartzell, 2000). This low selectivity is precisely what one might expect  
397 to evolve from a transporter that previously transported phospholipids. The finding that we can convert  
398 ANO1 into a protein capable of catalyzing PLS provides further support for this hypothesis for ANO1  
399 evolution. Like the ClC family, where a single glutamic acid residue can determine whether a protein is a  
400  $\text{H}^+$ - $\text{Cl}^-$  transporter or a  $\text{Cl}^-$  channel, here we show that a few amino acids can convert ANO1 into a protein  
401 that supports PLS activity. However, we have not yet been able to convert ANO6 into a  $\text{Cl}^-$  selective ion  
402 channel. It is likely that additional changes outside the SCR D are required to confer  $\text{Cl}^-$  selectivity. This  
403 may be also be explained by epistasis, where evolutionary trajectories are blocked by the accumulation of

neutral mutations that have no impact on the initial function (non-selective ion transport) but prevent acquisition of the new function (Cl<sup>-</sup> selectivity) (Breen et al., 2012; Bridgham et al., 2009). Yang et al. (2011) have reported that mutations of the last amino acid in the SCRD (Q559 in ANO6, K588 in ANO1) alters the ionic selectivity, but the changes are only 2-3-fold and do not shift selectivity from cation to anion.

Intriguingly, the *Saccharomyces* ANO homolog, Ist2p, has been shown to play a role in tethering the cortical ER to the plasma membrane, but it is not known whether this protein also has PLSase or ion channel activity. However, one might speculate wildly that Ist2p may play a role in transport of lipids from the ER to the plasma membrane, because tethering of the ER to the plasma membrane is important for the proper function of non-vesicular lipid transport (Holthuis and Menon, 2014) and deletion of Ist2p along with other ER-plasma membrane tethering proteins results in aberrant phosphatidylinositol 4-phosphate levels and localization (Manford et al., 2012; Stefan et al., 2011; Stefan et al., 2013; Wolf et al., 2012).

*Is ANO1 a PLSase?* ANO1 is well established as the pore forming unit of Ca<sup>2+</sup> activated Cl<sup>-</sup> channels (Caputo et al., 2008; Schroeder et al., 2008; Yang et al., 2008) and is incapable of rescuing PLS in cells with ANO6 disrupted (Suzuki et al., 2013b). However, our finding that the function of ANO1 can be converted by replacing a domain as small as 15 amino acids raises questions whether ANO1 might be a PLSase under appropriate conditions. Perhaps a missing subunit or regulatory enzyme could activate its PLSase activity. Alternatively, the SCRD may hold a vital interaction site for another component essential for this process or possess a key site of posttranscriptional modification required for activating this activity. In any case, it is clear that ANO1 function is intimately dependent on phospholipids (Terashima et al., 2013) and understanding the relationships of the ANOs to membrane lipids is certain to be a major research goal for many laboratories in the coming years.

## Materials and Methods

*cDNAs.* mANO1 (Uniprot Q8BHY3) and mANO6 (Uniprot Q6P9J9) tagged on the C-terminus with EGFP were provided by Dr. Uhtaek Oh, Seoul National University. For designing chimeras, mANO1 and mANO6 were aligned using MUSCLE (McWilliam et al., 2013). Chimeras were constructed using overlap extension PCR (Pont-Kingdon, 1997). Chimeras are named X-Y-X<sub>*i-j*</sub>, where X is the ANO paralog template whose amino acids numbered *i-j* are replaced with the aligned amino acids from ANO paralog Y. The alignment is shown in Figure 5-figure supplement 2. PCR primers were designed to engineer complementary overlapping sequences onto the junction-forming ends of PCR products that were subsequently assembled by PCR. PCR-based mutagenesis was used to generate mutations in one or a few amino acids. The protein coding region of all chimeras and mutants were sequenced.

*Clover-(His)<sub>6</sub>-LactC2.* A cDNA construct consisting of Clover fluorescent protein followed by a hexa-histidine tag and lactadherin-C2 (Clover-(His)<sub>6</sub>-LactC2) in the pET-28 bacterial expression vector was a generous gift from Dr. Leonid Chernomordik (NIH/NICHD). Rosetta2(DE3) BL21 *E.coli* (Novagen) were transformed with Clover-(His)<sub>6</sub>-LactC2 in pET28, grown in TB medium at 37 °C in 50 µg/ml kanamycin and 30 µg/ml chloramphenicol until the culture reached A<sub>600</sub> = 1. After addition of 1 mM IPTG, the culture was grown for 3 hrs at 28 °C. Cells were lysed in B-Per (Thermo Scientific) containing lysozyme, benzoase, and protease inhibitor cocktail III (Calbiochem). After centrifugation at 20,000g 10 min, Clover-(His)<sub>6</sub>-LactC2 was purified from the supernate on a 1-ml Talon cobalt affinity

column (Clontech). Stock solutions of 1 -3 mg/ml were stored in the elution buffer (150 mM imidazole pH 7 plus 0.02% NaN<sub>3</sub>) and were used at ~1 - 3 µg/ml.

*Patch clamp electrophysiology.* HEK293 cells were transfected with ~1 µg cDNA per 35 mm dish) using Fugene-9 (Roche Molecular Biochemicals, Indianapolis, IN). Single cells identified by EGFP fluorescence were patch clamped ~2 days after transfection. Transfected cells were identified on a Zeiss Axiovert microscope by EGFP fluorescence. Cells were voltage-clamped using conventional whole-cell patch-clamp techniques with an EPC-7 amplifier (HEKA). Fire-polished borosilicate glass patch pipettes were 3-5 MΩ. Experiments were conducted at ambient temperature (22-26°C). Because liquid junction potentials calculated using pClamp were predicted to be < 2 mV, no correction was made. The zero Ca<sup>2+</sup> pipet (intracellular) solution contained (mM): 146 CsCl, 2 MgCl<sub>2</sub>, 5 EGTA, 10 sucrose, 10 HEPES pH 7.3, adjusted with NMDG. The ~20 µM Ca<sup>2+</sup> pipet solution contained 5 mM Ca<sup>2+</sup>-EGTA. The 0.2 mM Ca<sup>2+</sup> solution was made by adding additional 0.2 mM CaCl<sub>2</sub> to the 20 µM Ca<sup>2+</sup> pipet solution. The standard extracellular solution contained (mM): 140 NaCl, 5 KCl, 2 CaCl<sub>2</sub>, 1 MgCl<sub>2</sub>, 15 glucose, 10 HEPES pH 7.4. For determination of ionic selectivity, the external solution contained 2 CaCl<sub>2</sub>, 1 MgCl<sub>2</sub>, 15 glucose, 10 HEPES pH 7.4, and various concentrations of NaCl, CsCl, or NMDG-Cl as indicated. The internal solution contained (mM): 150 NaCl (or CsCl), 1 MgCl<sub>2</sub>, 5 Ca-EGTA plus 0.2 CaCl<sub>2</sub>, and 10 HEPES pH 7.4. The osmolarity of each solution was adjusted to 300 mOsm by addition of mannitol. Relative permeabilities of cations (X) relative to Cl<sup>-</sup> were determined by measuring the changes in zero-current  $E_{rev}$  when the concentration of extracellular NaCl or CsCl was changed (“dilution potential” method) as previously described (Barry, 2006; Yu et al., 2012). Relative permeabilities were calculated from the shift in  $E_{rev}$  calculated using the Goldman-Hodgkin-Katz equation:

$$\Delta E_{rev} = 25.7 \ln[(X_o + Cl_i * P_{Cl}/P_{Na}) / (X_i + Cl_o * P_{Cl}/P_{Na})]$$
, where X is the cation and  $\Delta E_{rev}$  is the difference between  $E_{rev}$  with the test solution XCl and that observed with symmetrical solutions.

*Phospholipid scrambling.* Phospholipid scrambling (PLS) was assessed by live-cell imaging of the binding of Annexin-V conjugated to Alexa Fluor-568 (Invitrogen, “Annexin-V” diluted 1:200) or LactC2 fused to Clover fluorescent protein (Kay et al., 2012). PLS was measured in populations of intact HEK293 cells grown on glass coverslips mounted in Attofluor chambers (Invitrogen) and imaged at ambient temperature with a Zeiss confocal microscope using a 63X Plan-Aprochromat NA 1.4 objective. PtdSer exposure was measured by binding of Annexin-V-AlexaFluor-568 (543nm excitation; 560 nm long pass emission) or LactC2-Clover (488nm excitation, 500-530nm band pass emission). The bath solution contained (mM) 140 NaCl, 10 CaCl<sub>2</sub>, 10 Tris-HCl pH 7.4. PLS was stimulated by elevation of intracellular Ca<sup>2+</sup> using the Ca<sup>2+</sup> ionophore A23187 (10 µM). The most reproducible PLS was obtained by incubation of cells 5 min in A23187 in nominally zero-Ca<sup>2+</sup> solution followed by washout of A23187 and addition of 5 mM Ca<sup>2+</sup> to initiate PLS. We presume that the A23187 exposure in zero Ca<sup>2+</sup> depletes internal stores and that the readdition of Ca<sup>2+</sup> results in store-operated Ca<sup>2+</sup> entry that is more rapid than Ca<sup>2+</sup> entry through A23187 channels alone. In some experiments, PLS was stimulated by exposure to A23187 and Ca<sup>2+</sup> simultaneously. Sometimes SERCA inhibitors were included with no obvious effect. Scrambling was quantified by measuring the increase in Annexin-V fluorescence in EGFP-expressing cells by creating a binary mask from the EGFP channel for each Annexin-V-Alexa-568 frame in the time series using Fiji Image-J 1.49. The raw integrated density was then calculated by adding the intensity of all pixels in the unmasked area.

Binding of Annexin-V-AlexaFluor-568 to patch-clamped cells during voltage-clamp recording was imaged with a wide-field Zeiss Axiovert 100 microscope using a 40X NA 0.6 LD-Acroplan objective. Images were acquired with an Orca-FLASH 4.0 digital CMOS camera (C11440, Hamamatsu) controlled by Metamorph 7.8 software (Molecular Devices). Annexin-V-AlexaFluor-568 was added to the normal extracellular solution before patch clamping the cell. After whole-cell recording was established with an intracellular solution containing either zero, 20  $\mu$ M, or 200  $\mu$ M free  $\text{Ca}^{2+}$  the accumulation of Annexin-V on the plasma membrane was imaged at 1-min intervals synchronously with voltage clamp recording.

*Immunostaining and Antibodies.* Stable ANO6-FLAG<sub>3X</sub> cells were fixed on glass coverslips in 4% PFA for 10 min at room temperature, permeabilized with 1.5% Tritonx-100 and stained with anti-FLAG M2 antibody (Sigma-Aldrich) for two hours at room temperature. Coverslips were washed and stained with anti-mouse-Alexa-488 secondary and Alexa-633 conjugated phalloidin (1:1000, Molecular Probes). Western blot analysis was performed on protein lysates using anti-FLAG M2 antibody and anti-GAPDH (Millipore) followed by incubation with HRP conjugated anti-mouse secondary (BioRad).

*Divergence Analysis.* Type-II divergence was determined using DIVERGE 3.0 (<http://xungulab.com/software.html>) (Gu, 2006; Gu et al., 2013). Sequences used for the DIVERGE analysis are listed in Figure 5-figure supplement 1. Sequences were curated, divergent N-terminal and C-terminal sequences were deleted, and the sequences aligned using MUSCLE. For plotting, the site-specific posterior ratios for Type II divergence were binned across a window of 15 amino acids and normalized to the maximum value.

*Homology Models.* We created homology models of ANO6 based on nhTMEM16 (Brunner et al., 2014). mANO6 sequence was submitted to the Phyre2 Protein Fold Recognition Server (Kelley and Sternberg, 2009). mANO6 (truncated to 833 residues by deleting the extreme N- and C- termini) was aligned to the nhTMEM16 sequence extracted from PDB ID 4WIT (674 residues). These two sequences share 23% identity and 37.4% similarity (calculated by the BLSM62 algorithm). A total of 12 gaps were introduced, primarily at the N- and C-termini and in loops between secondary structural elements. Secondary structure prediction was incorporated into the alignment for Phyre2 (and all of the other modeling servers used for comparison including Swiss-Model and Tasser). There are no gaps in or near the SCRD, with the nearest gaps located in extracellular loops between helices 3 and 4 (2 residue gap 24 residues away) and between helices 4 and 5 (1 residue gap 22 residues away). While overall alignment and homology model generation would benefit from a template with greater sequence identity, all modeling servers reported high confidence in the generated models with no variation in the placement of the SCRD between models. Model geometry was minimized and the model subjected to 500 steps of geometry idealization and energy minimization using Phenix (Adams et al., 2010). The overall RMSD of  $\text{Ca}$  atoms in the final alignment was 1.485 Å with a Q-score of 0.667 (calculated by UCSF Chimera).

*Analysis of Data.* Electrophysiological traces were analyzed with Clampfit 9 (Molecular Devices). Fluorescence intensity was analyzed with MetaMorph 7.8 and Fiji Image-J 1.49. Data are presented as mean  $\pm$  SEM. Statistical difference between means was evaluated by two-tailed t-test. Statistical significance was assumed at  $p < 0.05$ .

## Acknowledgements:

Supported by NIH grants GM60448-12 and EY114852-11 to HCH. Jarred Whitlock was supported by an NIH Training Grant 5T32GM008367-25. This research project was supported in part by the Emory University Integrated Cellular Imaging Microscopy Core

## References

- Acharya, U., M.B. Edwards, R.A. Jorquera, H. Silva, K. Nagashima, P. Labarca, and J.K. Acharya. 2006. *Drosophila melanogaster* Scramblases modulate synaptic transmission. *J Cell Biol.* 173:69-82. doi:10.1083/jcb.200506159.
- Adams, P.D., P.V. Afonine, G. Bunkoczi, V.B. Chen, I.W. Davis, N. Echols, J.J. Headd, L.W. Hung, G.J. Kapral, R.W. Grosse-Kunstleve, A.J. McCoy, N.W. Moriarty, R. Oeffner, R.J. Read, D.C. Richardson, J.S. Richardson, T.C. Terwilliger, and P.H. Zwart. 2010. PHENIX: a comprehensive Python-based system for macromolecular structure solution. *Acta crystallographica. Section D, Biological crystallography.* 66:213-221. doi:10.1107/S0907444909052925.
- Adomaviciene, A., K.J. Smith, H. Garnett, and P. Tammaro. 2013. Putative pore-loops of TMEM16/anoctamin channels affect channel density in cell membranes. *J Physiol.* 591:3487-3505. doi:10.1113/jphysiol.2013.251660.
- Almaca, J., Y. Tian, F. Aldehni, J. Ousingsawat, P. Kongsuphol, J.R. Rock, B.D. Harfe, R. Schreiber, and K. Kunzelmann. 2009. TMEM16 proteins produce volume-regulated chloride currents that are reduced in mice lacking TMEM16A. *J Biol Chem.* 284:28571-28578. doi:M109.010074 [pii] 10.1074/jbc.M109.010074.
- Baldrige, R.D., and T.R. Graham. 2013. Two-gate mechanism for phospholipid selection and transport by type IV P-type ATPases. *Proc Natl Acad Sci U S A.* 110:E358-367. doi:10.1073/pnas.1216948110.
- Barry, P. 2006. The reliability of relative anion-cation permeabilities deduced from reversal (Dilution) potential measurements in ion channel studies. *Cell Biochemistry and Biophysics.* 46:143-154. doi:10.1385/cbb:46:2:143.
- Basse, F., J.G. Stout, P.J. Sims, and T. Wiedmer. 1996. Isolation of an erythrocyte membrane protein that mediates Ca<sup>2+</sup>-dependent transbilayer movement of phospholipid. *J Biol Chem.* 271:17205-17210. doi, <http://www.ncbi.nlm.nih.gov/pubmed/8663431>.
- Bevers, E.M., and P.L. Williamson. 2010. Phospholipid scramblase: an update. *FEBS Lett.* 584:2724-2730. doi:10.1016/j.febslet.2010.03.020.
- Bigay, J., and B. Antonny. 2012. Curvature, lipid packing, and electrostatics of membrane organelles: defining cellular territories in determining specificity. *Developmental cell.* 23:886-895. doi:10.1016/j.devcel.2012.10.009.
- Bill, A., M.O. Popa, M.T. van Diepen, A. Gutierrez, S. Lilley, M. Velkova, K. Acheson, H. Choudhury, N.A. Renaud, D.S. Auld, M. Gosling, P.J. Groot-Kormelink, and L.A. Gaither. 2015. Variomics Screen Identifies the Re-entrant Loop of the Calcium-activated Chloride Channel ANO1 That Facilitates Channel Activation. *J Biol Chem.* 290:889-903. doi:10.1074/jbc.M114.618140.
- Borst, P., N. Zelcer, and A. van Helvoort. 2000. ABC transporters in lipid transport. *Biochim Biophys Acta.* 1486:128-144. doi, <http://www.ncbi.nlm.nih.gov/pubmed/10856718>.
- Breen, M.S., C. Kemena, P.K. Vlasov, C. Notredame, and F.A. Kondrashov. 2012. Epistasis as the primary factor in molecular evolution. *Nature.* 490:535-538. doi:10.1038/nature11510.
- Bretscher, M.S. 1972. Asymmetrical lipid bilayer structure for biological membranes. *Nature: New biology.* 236:11-12. doi, <http://www.ncbi.nlm.nih.gov/pubmed/4502419>.
- Bridgham, J.T., E.A. Ortlund, and J.W. Thornton. 2009. An epistatic ratchet constrains the direction of glucocorticoid receptor evolution. *Nature.* 461:515-519. doi:10.1038/nature08249.

- Brunner, J.D., N.K. Lim, S. Schenck, A. Duerst, and R. Dutzler. 2014. X-ray structure of a calcium-activated TMEM16 lipid scramblase. *Nature*. 516:207-212. doi:10.1038/nature13984.
- Caputo, A., E. Caci, L. Ferrera, N. Pedemonte, C. Barsanti, E. Sondo, U. Pfeffer, R. Ravazzolo, O. Zegarra-Moran, and L.J.V. Galletta. 2008. TMEM16A, A Membrane Protein Associated With Calcium-Dependent Chloride Channel Activity. *Science*. 322:590-594. doi, <http://www.sciencemag.org/cgi/content/abstract/1163518v1>.
- Comfurius, P., P. Williamson, E.F. Smeets, R.A. Schlegel, E.M. Bevers, and R.F. Zwaal. 1996. Reconstitution of phospholipid scramblase activity from human blood platelets. *Biochemistry*. 35:7631-7634. doi:10.1021/bi9606859.
- Dawson, D.C., S.S. Smith, and M.K. Mansoura. 1999. CFTR: mechanism of anion conduction. *Physiological Reviews*. 79:S47-S75. doi.
- Duran, C., and H.C. Hartzell. 2011. Physiological roles and diseases of TMEM16/anoctamin proteins: are they all chloride channels? *Acta Pharmacol Sin*. 32:685-692. doi:aps201148 [pii] 10.1038/aps.2011.48.
- Duran, C., C.H. Thompson, Q. Xiao, and H.C. Hartzell. 2010. Chloride channels: often enigmatic, rarely predictable. *Annu Rev Physiol*. 72:95-121. doi:10.1146/annurev-physiol-021909-135811.
- Emoto, K., N. Toyama-Sorimachi, H. Karasuyama, K. Inoue, and M. Umeda. 1997. Exposure of phosphatidylethanolamine on the surface of apoptotic cells. *Exp Cell Res*. 232:430-434. doi:10.1006/excr.1997.3521.
- Fadeel, B., and D. Xue. 2009. The ins and outs of phospholipid asymmetry in the plasma membrane: roles in health and disease. *Crit Rev Biochem Mol Biol*. 44:264-277. doi:10.1080/10409230903193307.
- Fadok, V.A., A. de Cathelineau, D.L. Daleke, P.M. Henson, and D.L. Bratton. 2001. Loss of phospholipid asymmetry and surface exposure of phosphatidylserine is required for phagocytosis of apoptotic cells by macrophages and fibroblasts. *J Biol Chem*. 276:1071-1077. doi:10.1074/jbc.M003649200.
- Fadok, V.A., D.R. Voelker, P.A. Campbell, J.J. Cohen, D.L. Bratton, and P.M. Henson. 1992. Exposure of phosphatidylserine on the surface of apoptotic lymphocytes triggers specific recognition and removal by macrophages. *J Immunol*. 148:2207-2216. doi, <http://www.ncbi.nlm.nih.gov/pubmed/1545126>.
- Fairn, G.D., M. Hermansson, P. Somerharju, and S. Grinstein. 2011. Phosphatidylserine is polarized and required for proper Cdc42 localization and for development of cell polarity. *Nat Cell Biol*. 13:1424-1430. doi:10.1038/ncb2351.
- Gadsby, D.C., P. Vergani, and L. Csanady. 2006. The ABC protein turned chloride channel whose failure causes cystic fibrosis. *Nature*. 440:477-483. doi, PM:16554808.
- Goren, M.A., T. Morizumi, I. Menon, J.S. Joseph, J.S. Dittman, V. Cherezov, R.C. Stevens, O.P. Ernst, and A.K. Menon. 2014. Constitutive phospholipid scramblase activity of a G protein-coupled receptor. *Nature communications*. 5:5115. doi:10.1038/ncomms6115.
- Graham, T.R., and M.M. Kozlov. 2010. Interplay of proteins and lipids in generating membrane curvature. *Curr Opin Cell Biol*. 22:430-436. doi:10.1016/j.ceb.2010.05.002.
- Grubb, S., K.A. Poulsen, C.A. Juul, T. Kyed, T.K. Klausen, E.H. Larsen, and E.K. Hoffmann. 2013. TMEM16F (Anoctamin 6), an anion channel of delayed Ca(2+) activation. *J Gen Physiol*. 141:585-600. doi:10.1085/jgp.201210861.
- Gu, X. 2006. A simple statistical method for estimating type-II (cluster-specific) functional divergence of protein sequences. *Molecular biology and evolution*. 23:1937-1945. doi:10.1093/molbev/msl056.
- Gu, X., Y. Zou, Z. Su, W. Huang, Z. Zhou, Z. Arendsee, and Y. Zeng. 2013. An update of DIVERGE software for functional divergence analysis of protein family. *Molecular biology and evolution*. 30:1713-1719. doi:10.1093/molbev/mst069.
- Harper, M.T., and A.W. Poole. 2013. Chloride channels are necessary for full platelet phosphatidylserine exposure and procoagulant activity. *Cell death & disease*. 4:e969. doi:10.1038/cddis.2013.495.

- Harre, U., H. Keppeler, N. Ipseiz, A. Derer, K. Poller, M. Aigner, G. Schett, M. Herrmann, and K. Lauber. 2012. Moonlighting osteoclasts as undertakers of apoptotic cells. *Autoimmunity*. 45:612-619. doi:10.3109/08916934.2012.719950.
- Hartzell, H.C., K. Yu, Q. Xiao, L.T. Chien, and Z. Qu. 2009. Anoctamin / TMEM16 family members are  $\text{Ca}^{2+}$ -activated  $\text{Cl}^-$  channels. *The Journal of Physiology*. 587.10:2127-2139. doi, PM:19015192.
- Helming, L., and S. Gordon. 2009. Molecular mediators of macrophage fusion. *Trends Cell Biol*. 19:514-522. doi:10.1016/j.tcb.2009.07.005.
- Hochreiter-Hufford, A.E., C.S. Lee, J.M. Kinchen, J.D. Sokolowski, S. Arandjelovic, J.A. Call, A.L. Klibanov, Z. Yan, J.W. Mandell, and K.S. Ravichandran. 2013. Phosphatidylserine receptor BAI1 and apoptotic cells as new promoters of myoblast fusion. *Nature*. 497:263-267. doi:10.1038/nature12135.
- Holthuis, J.C., and A.K. Menon. 2014. Lipid landscapes and pipelines in membrane homeostasis. *Nature*. 510:48-57. doi:10.1038/nature13474.
- Hosseini, A.S., H. Zheng, and J. Gao. 2014. Understanding Lipid Recognition by Protein-Mimicking Cyclic Peptides. *Tetrahedron*. 70:7632-7638. doi:10.1016/j.tet.2014.07.104.
- Hou, J., Y. Fu, J. Zhou, W. Li, R. Xie, F. Cao, G.E. Gilbert, and J. Shi. 2011. Lactadherin functions as a probe for phosphatidylserine exposure and as an anticoagulant in the study of stored platelets. *Vox sanguinis*. 100:187-195. doi:10.1111/j.1423-0410.2010.01375.x.
- Huppertz, B., C. Bartz, and M. Kokozidou. 2006. Trophoblast fusion: fusogenic proteins, syncytins and ADAMs, and other prerequisites for syncytial fusion. *Micron*. 37:509-517. doi:10.1016/j.micron.2005.12.011.
- Jeong, J., and I.M. Conboy. 2011. Phosphatidylserine directly and positively regulates fusion of myoblasts into myotubes. *Biochem Biophys Res Commun*. 414:9-13. doi:10.1016/j.bbrc.2011.08.128.
- Jordan, I.K., K.C. Kota, G. Cui, C.H. Thompson, and N.A. McCarty. 2008. Evolutionary and functional divergence between the cystic fibrosis transmembrane conductance regulator and related ATP-binding cassette transporters. *Proc Natl Acad Sci U S A*. 105:18865-18870. doi:10.1073/pnas.0806306105.
- Juul, C.A., S. Grubb, K.A. Poulsen, T. Kyed, N. Hashem, I.H. Lambert, E.H. Larsen, and E.K. Hoffmann. 2014. Anoctamin 6 differs from VRAC and VSOAC but is involved in apoptosis and supports volume regulation in the presence of  $\text{Ca}^{2+}$ . *Pflugers Arch*. 466:1899-1910. doi:10.1007/s00424-013-1428-4.
- Kastl, K., M. Ross, V. Gerke, and C. Steinem. 2002. Kinetics and thermodynamics of annexin A1 binding to solid-supported membranes: a QCM study. *Biochemistry*. 41:10087-10094. doi, <http://www.ncbi.nlm.nih.gov/pubmed/12146973>.
- Kay, J.G., and S. Grinstein. 2011. Sensing phosphatidylserine in cellular membranes. *Sensors*. 11:1744-1755. doi:10.3390/s110201744.
- Kay, J.G., and S. Grinstein. 2013. Phosphatidylserine-mediated cellular signaling. *Adv Exp Med Biol*. 991:177-193. doi:10.1007/978-94-007-6331-9\_10.
- Kay, J.G., M. Koivusalo, X. Ma, T. Wohland, and S. Grinstein. 2012. Phosphatidylserine dynamics in cellular membranes. *Mol Biol Cell*. 23:2198-2212. doi:10.1091/mbc.E11-11-0936.
- Kelley, L.A., and M.J. Sternberg. 2009. Protein structure prediction on the Web: a case study using the Phyre server. *Nat Protoc*. 4:363-371. doi:10.1038/nprot.2009.2.
- Kmit, A., R. van Kruchten, J. Ousingsawat, N.J. Mattheij, B. Senden-Gijsbers, J.W. Heemskerk, R. Schreiber, E.M. Bevers, and K. Kunzelmann. 2013. Calcium-activated and apoptotic phospholipid scrambling induced by Ano6 can occur independently of Ano6 ion currents. *Cell death & disease*. 4:e611. doi:10.1038/cddis.2013.135.
- Kunzelmann, K., B. Nilius, G. Owsianik, R. Schreiber, J. Ousingsawat, L. Sirianant, P. Wanitchakool, E.M. Bevers, and J.W. Heemskerk. 2014. Molecular functions of anoctamin 6 (TMEM16F): a



chloride channel, cation channel, or phospholipid scramblase? *Pflugers Arch.* 466:407-414. doi:10.1007/s00424-013-1305-1.

Lhermusier, T., H. Chap, and B. Payrastre. 2011. Platelet membrane phospholipid asymmetry: from the characterization of a scramblase activity to the identification of an essential protein mutated in Scott syndrome. *J Thromb Haemost.* 9:1883-1891. doi:10.1111/j.1538-7836.2011.04478.x.

Lisal, J., and M. Maduke. 2008. The CIC-0 chloride channel is a 'broken' Cl<sup>-</sup>/H<sup>+</sup> antiporter. *Nat. Struct. Mol. Biol.* 15:805-810. doi, PM:18641661.

Liu, X., S.S. Smith, and D.C. Dawson. 2003. CFTR: what's it like inside the pore?. [Review] [37 refs]. *Journal of Experimental Zoology. Part A, Comparative Experimental Biology.* 300:69-75. doi.

Lopez-Marques, R.L., L. Theorin, M.G. Palmgren, and T.G. Pomorski. 2014. P4-ATPases: lipid flippases in cell membranes. *Pflugers Arch.* 466:1227-1240. doi:10.1007/s00424-013-1363-4.

Malvezzi, M., M. Chalal, R. Janjusevic, A. Picollo, H. Terashima, A.K. Menon, and A. Accardi. 2013. Ca<sup>2+</sup>-dependent phospholipid scrambling by a reconstituted TMEM16 ion channel. *Nat. Commun.* 4:2367. doi:10.1038/ncomms3367.

Manford, A.G., C.J. Stefan, H.L. Yuan, J.A. Macgurn, and S.D. Emr. 2012. ER-to-plasma membrane tethering proteins regulate cell signaling and ER morphology. *Developmental cell.* 23:1129-1140. doi:10.1016/j.devcel.2012.11.004.

Martins, J.R., D. Faria, P. Kongsuphol, B. Reisch, R. Schreiber, and K. Kunzelmann. 2011. Anoctamin 6 is an essential component of the outwardly rectifying chloride channel. *Proc Natl Acad Sci U S A.* 108:18168-18172. doi:10.1073/pnas.1108094108.

McWilliam, H., W. Li, M. Uludag, S. Squizzato, Y.M. Park, N. Buso, A.P. Cowley, and R. Lopez. 2013. Analysis Tool Web Services from the EMBL-EBI. *Nucleic Acids Res.* 41:W597-600. doi:10.1093/nar/gkt376.

Miller, C. 2006. CIC chloride channels viewed through a transporter lens. *Nature.* 440:484-489. doi, PM:16554809.

Miller, C. 2010. CFTR: break a pump, make a channel. *Proc Natl Acad Sci U S A.* 107:959-960. doi:10.1073/pnas.0913576107.

Oh, S.J., S.J. Hwang, J. Jung, K. Yu, J. Kim, J.Y. Choi, H.C. Hartzell, E.J. Roh, and C.J. Lee. 2013. MONNA, a potent and selective blocker for transmembrane protein with unknown function 16/anoctamin-1. *Mol Pharmacol.* 84:726-735. doi:10.1124/mol.113.087502.

Ory, S., M. Ceridono, F. Momboisse, S. Houy, S. Chasserot-Golaz, D. Heintz, V. Calco, A.M. Haeberle, F.A. Espinoza, P.J. Sims, Y. Bailly, M.F. Bader, and S. Gasman. 2013. Phospholipid scramblase-1-induced lipid reorganization regulates compensatory endocytosis in neuroendocrine cells. *J Neurosci.* 33:3545-3556. doi:10.1523/JNEUROSCI.3654-12.2013.

Pajcini, K.V., J.H. Pomerantz, O. Alkan, R. Doyonnas, and H.M. Blau. 2008. Myoblasts and macrophages share molecular components that contribute to cell-cell fusion. *J Cell Biol.* 180:1005-1019. doi:10.1083/jcb.200707191.

Panatala, R., H. Hennrich, and J.C. Holthuis. 2015. Inner workings and biological impact of phospholipid flippases. *J Cell Sci.* doi:10.1242/jcs.102715.

Pedemonte, N., and L.J. Galletta. 2014. Structure and Function of TMEM16 Proteins (Anoctamins). *Physiol Rev.* 94:419-459. doi:10.1152/physrev.00039.2011.

Picollo, A., M. Malvezzi, and A. Accardi. 2015. TMEM16 Proteins: Unknown Structure and Confusing Functions. *J Mol Biol.* 427:94-105. doi:10.1016/j.jmb.2014.09.028.

Pomorski, T., and A.K. Menon. 2006. Lipid flippases and their biological functions. *Cell Mol Life Sci.* 63:2908-2921. doi:10.1007/s00018-006-6167-7.

Pont-Kingdon, G. 1997. Creation of chimeric junctions, deletions, and insertions by PCR. *Methods Mol Biol.* 67:167-172. doi, http://www.ncbi.nlm.nih.gov/pubmed/9031140.

Qu, Z., and H.C. Hartzell. 2000. Anion permeation in Ca<sup>2+</sup>-activated Cl<sup>-</sup> channels. *J. Gen. Physiol.* 116:825-844. doi, PM:11099350.

- Riddell, M.R., B. Winkler-Lowen, Y. Jiang, S.T. Davidge, and L.J. Guilbert. 2013. Pleiotropic actions of forskolin result in phosphatidylserine exposure in primary trophoblasts. *PLoS One*. 8:e81273. doi:10.1371/journal.pone.0081273.
- Ruppersburg, C.C., and H.C. Hartzell. 2014. The Ca<sup>2+</sup>-activated Cl<sup>-</sup> channel ANO1/TMEM16A regulates primary ciliogenesis. *Mol Biol Cell*. 25:1793-1807. doi:10.1091/mbc.E13-10-0599.
- Sahu, S.K., S.N. Gummadi, N. Manoj, and G.K. Aradhyam. 2007. Phospholipid scramblases: an overview. *Arch Biochem Biophys*. 462:103-114. doi:10.1016/j.abb.2007.04.002.
- Sanyal, S., and A.K. Menon. 2009. Flipping lipids: why an' what's the reason for? *ACS chemical biology*. 4:895-909. doi:10.1021/cb900163d.
- Schoenwaelder, S.M., Y. Yuan, E.C. Josefsson, M.J. White, Y. Yao, K.D. Mason, L.A. O'Reilly, K.J. Henley, A. Ono, S. Hsiao, A. Willcox, A.W. Roberts, D.C. Huang, H.H. Salem, B.T. Kile, and S.P. Jackson. 2009. Two distinct pathways regulate platelet phosphatidylserine exposure and procoagulant function. *Blood*. 114:663-666. doi:10.1182/blood-2009-01-200345.
- Schroeder, B.C., T. Cheng, Y.N. Jan, and L.Y. Jan. 2008. Expression Cloning of TMEM16A as a Calcium-Activated Chloride Channel Subunit. *Cell*. 134:1019-1029. doi.
- Shi, J., Y. Shi, L.N. Waehrens, J.T. Rasmussen, C.W. Heegaard, and G.E. Gilbert. 2006. Lactadherin detects early phosphatidylserine exposure on immortalized leukemia cells undergoing programmed cell death. *Cytometry. Part A : the journal of the International Society for Analytical Cytology*. 69:1193-1201. doi:10.1002/cyto.a.20345.
- Shimizu, T., T. Iehara, K. Sato, T. Fujii, H. Sakai, and Y. Okada. 2013. TMEM16F is a component of a Ca<sup>2+</sup>-activated Cl<sup>-</sup> channel but not a volume-sensitive outwardly rectifying Cl<sup>-</sup> channel. *Am J Physiol Cell Physiol*. 304:C748-759. doi:10.1152/ajpcell.00228.2012.
- Shin, N.Y., H. Choi, L. Neff, Y. Wu, H. Saito, S.M. Ferguson, P. De Camilli, and R. Baron. 2014. Dynamin and endocytosis are required for the fusion of osteoclasts and myoblasts. *J Cell Biol*. 207:73-89. doi:10.1083/jcb.201401137.
- Stefan, C.J., A.G. Manford, D. Baird, J. Yamada-Hanff, Y. Mao, and S.D. Emr. 2011. Osh proteins regulate phosphoinositide metabolism at ER-plasma membrane contact sites. *Cell*. 144:389-401. doi:10.1016/j.cell.2010.12.034.
- Stefan, C.J., A.G. Manford, and S.D. Emr. 2013. ER-PM connections: sites of information transfer and inter-organelle communication. *Curr Opin Cell Biol*. 25:434-442. doi:10.1016/j.ceb.2013.02.020.
- Suetsugu, S., S. Kurisu, and T. Takenawa. 2014. Dynamic Shaping of Cellular Membranes by Phospholipids and Membrane-Deforming Proteins. *Physiol Rev*. 94:1219-1248. doi:10.1152/physrev.00040.2013.
- Suh, B.C., and B. Hille. 2008. PIP2 is a necessary cofactor for ion channel function: how and why? *Annual review of biophysics*. 37:175-195. doi:10.1146/annurev.biophys.37.032807.125859.
- Suzuki, J., D.P. Denning, E. Imanishi, H.R. Horvitz, and S. Nagata. 2013a. Xk-related protein 8 and CED-8 promote phosphatidylserine exposure in apoptotic cells. *Science*. 341:403-406. doi:10.1126/science.1236758.
- Suzuki, J., T. Fujii, T. Imao, K. Ishihara, H. Kuba, and S. Nagata. 2013b. Calcium-dependent phospholipid scramblase activity of TMEM16 protein family members. *J Biol Chem*. 288:13305-13316. doi:10.1074/jbc.M113.457937.
- Suzuki, J., E. Imanishi, and S. Nagata. 2014. Exposure of phosphatidylserine by Xk-related protein family members during apoptosis. *J Biol Chem*. 289:30257-30267. doi:10.1074/jbc.M114.583419.
- Suzuki, J., M. Umeda, P.J. Sims, and S. Nagata. 2010. Calcium-dependent phospholipid scrambling by TMEM16F. *Nature*. 468:834-838. doi:nature09583 [pii] 10.1038/nature09583.
- Szteyn, K., E. Schmid, M.K. Nurbaeva, W. Yang, P. Munzer, K. Kunzelmann, F. Lang, and E. Shumilina. 2012. Expression and functional significance of the Ca(2+)-activated Cl(-) channel ANO6 in dendritic cells. *Cell Physiol Biochem*. 30:1319-1332. doi:10.1159/000343321.

- Terashima, H., A. Picollo, and A. Accardi. 2013. Purified TMEM16A is sufficient to form  $\text{Ca}^{2+}$ -activated Cl<sup>-</sup> channels. *Proceedings of the National Academy of Sciences of the United States of America*. 110:19354-19359. doi:DOI 10.1073/pnas.1312014110.
- Tien, J., C.J. Peters, X.M. Wong, T. Cheng, Y.N. Jan, L.Y. Jan, and H. Yang. 2014. A comprehensive search for calcium binding sites critical for TMEM16A calcium-activated chloride channel activity. *eLife*. 3. doi:10.7554/eLife.02772.
- Tyurin, V.A., Y.Y. Tyurina, P.M. Kochanek, R. Hamilton, S.T. DeKosky, J.S. Greenberger, H. Bayir, and V.E. Kagan. 2008. Oxidative lipidomics of programmed cell death. *Methods Enzymol*. 442:375-393. doi:10.1016/S0076-6879(08)01419-5.
- van Meer, G. 2011. Dynamic transbilayer lipid asymmetry. *Cold Spring Harbor perspectives in biology*. 3. doi:10.1101/cshperspect.a004671.
- Verhoven, B., R.A. Schlegel, and P. Williamson. 1995. Mechanisms of phosphatidylserine exposure, a phagocyte recognition signal, on apoptotic T lymphocytes. *J Exp Med*. 182:1597-1601. doi, <http://www.ncbi.nlm.nih.gov/pubmed/7595231>.
- Verma, S.K., E. Leikina, K. Melikov, and L.V. Chernomordik. 2014. Late stages of the synchronized macrophage fusion in osteoclast formation depend on dynamin. *Biochem J*. 464:293-300. doi:10.1042/BJ20141233.
- Wolf, W., A. Kilic, B. Schrul, H. Lorenz, B. Schwappach, and M. Seedorf. 2012. Yeast Ist2 recruits the endoplasmic reticulum to the plasma membrane and creates a ribosome-free membrane microcompartment. *PLoS One*. 7:e39703. doi:10.1371/journal.pone.0039703.
- Xiao, Q., K. Yu, P. Perez-Cornejo, Y. Cui, J. Arreola, and H.C. Hartzell. 2011. Voltage- and calcium-dependent gating of TMEM16A/Ano1 chloride channels are physically coupled by the first intracellular loop. *Proc. Natl. Acad. Sci*. 108:8891-8896. doi:10.1073/pnas.1102147108.
- Xu, P., R.D. Baldridge, R.J. Chi, C.G. Burd, and T.R. Graham. 2013. Phosphatidylserine flipping enhances membrane curvature and negative charge required for vesicular transport. *J Cell Biol*. 202:875-886. doi:10.1083/jcb.201305094.
- Yang, H., T. Jin, T. Cheng, Y.N. Jan, and L.Y. Jan. 2011. Scan: A Novel Small-Conductance  $\text{Ca}^{2+}$ -Activated Non-Selective Cation Channel Encoded by TMEM16F. *Biophys. J*. 100:259a. doi.
- Yang, H., A. Kim, T. David, D. Palmer, T. Jin, J. Tien, F. Huang, T. Cheng, S.R. Coughlin, Y.N. Jan, and L.Y. Jan. 2012. TMEM16F Forms a  $\text{Ca}^{2+}$ -Activated Cation Channel Required for Lipid Scrambling in Platelets during Blood Coagulation. *Cell*. 151:111-122. doi:10.1016/j.cell.2012.07.036
- S0092-8674(12)01104-X [pii].
- Yang, Y.D., H. Cho, J.Y. Koo, M.H. Tak, Y. Cho, W.S. Shim, S.P. Park, J. Lee, B. Lee, B.M. Kim, R. Raouf, Y.K. Shin, and U. Oh. 2008. TMEM16A confers receptor-activated calcium-dependent chloride conductance. *Nature*. 455:1210-1215. doi, <http://dx.doi.org/10.1038/nature07313>.
- Yu, K., C. Duran, Z. Qu, Y.Y. Cui, and H.C. Hartzell. 2012. Explaining calcium-dependent gating of anoctamin-1 chloride channels requires a revised topology. *Circ Res*. 110:990-999. doi:CIRCRESAHA.112.264440 [pii]
- 10.1161/CIRCRESAHA.112.264440.
- Yu, K., J. Zhu, Z. Qu, Y.Y. Cui, and H.C. Hartzell. 2014. Activation of the Ano1 (TMEM16A) chloride channel by calcium is not mediated by calmodulin. *J Gen Physiol*. 143:253-267. doi:10.1085/jgp.201311047.
- Zwaal, R.F., P. Comfurius, and E.M. Bevers. 1998. Lipid-protein interactions in blood coagulation. *Biochim Biophys Acta*. 1376:433-453. doi, <http://www.ncbi.nlm.nih.gov/pubmed/9805008>.

817 **Figure 1.** Expression of ANO6 in HEK cells stimulates  $\text{Ca}^{2+}$ -dependent phospholipid scrambling. (A.)  
818 Images of HEK cells stably transfected with ANO6-FLAG<sub>3X</sub> fixed and stained with anti-FLAG (green)  
819 and phalloidin (magenta). (B.-D.) Images of live cells after exposure to 10  $\mu\text{M}$  A23187 in zero- $\text{Ca}^{2+}$   
820 solution for 5 min followed by solution containing 5 mM  $\text{Ca}^{2+}$  and 3  $\mu\text{g/ml}$  LactC2-Clover for 12 min as  
821 described in Methods. Green channel: LactC2-Clover. DIC channel: differential interference contrast. (B.)  
822 HEK cells stably expressing ANO6-FLAG<sub>3X</sub>. (C.) Parental HEK cells not expressing ANO6. (D.) HEK  
823 cells stably transfected with ANO1-FLAG<sub>3X</sub>. (E.) A23187 in zero  $\text{Ca}^{2+}$  does not stimulate LactC2  
824 binding. The first two panels show LactC2-Clover binding in cells incubated in A23187 in zero  $\text{Ca}^{2+}$   
825 containing LactC2 for 15 min. The second two panels show the same cells 10 min after adding 5 mM  
826  $\text{Ca}^{2+}$ . (F.) Level of expression of ANO1 and ANO6 in stably expressing HEK cells. Extracts of cells in B-  
827 D were immunoblotted with anti-FLAG and anti-GAPDH to quantify protein expression. (G.) Numbers  
828 of cells binding Annexin-V (“scrambled”) or not binding Annexin-V (“not scrambled”) for parental HEK  
829 cells, ANO6-FLAG<sub>3X</sub>, and ANO1-FLAG<sub>3X</sub> expressing cells. (H.) Time course of Annexin-V and LactC2  
830 binding to HEK cells expressing ANO6-FLAG<sub>3X</sub>. Images of the same field of 30 – 100 cells were  
831 acquired at ~20 sec intervals. Annexin-V: mean  $\pm$  SEM of 7 independent experiments, LactC2: mean  $\pm$   
832 SEM of 5 independent experiments. Means at the end of the recordings were normalized to 1. Scale bars  
833 = 20  $\mu\text{m}$ .

835 **Figure 2.** Characteristics of phospholipid scrambling linked to ANO6. Intracellular  $\text{Ca}^{2+}$  was elevated by  
836 A23187, as in Figure 1, in polyclonal lines of HEK cells expressing (A.) ANO1-EGFP or (B.) ANO6-  
837 EGFP. (C.) The relationship between ANO6-EGFP expression (mean EGFP pixel density of each cell)  
838 and AnnexinV-Alexa568 binding (mean pixel density in the Annexin-V channel masked by the EGFP  
839 channel). The line is the best fit to a straight line with Pearson’s correlation coefficient  $r = 0.84$ . (D.)  
840 Examples of the time course of Annexin-V binding to 5 individual cells in a typical experiment. The  
841 numbers at the end of the trace represent the relative EGFP density of the cell and  $\tau$  is the time constant of  
842 a mono-exponential fit (light black line) of the data.

844 **Figure 3.** ANO6 current activates coincidentally with PLS. HEK cells transiently expressing ANO6-EGFP  
845 were patch clamped in the presence of Annexin-V-Alexa-568 in the bath. The EGFP fluorescence image  
846 was obtained before establishing whole-cell recording and  $F_0$  was determined immediately after  
847 establishing whole-cell recording. Annexin-V fluorescence images were acquired immediately after  
848 obtaining each I-V curve by voltage clamp at one minute intervals. The patch pipet contained 200 $\mu\text{M}$  free  
849  $\text{Ca}^{2+}$ . I-V curves were obtained by voltage steps from -100mV to +100 mV in 20 mV increments. (A)  
850 Representative images and currents of one of 20 experiments. The first image shows ANO6-EGFP  
851 fluorescence. The patch pipet can be seen entering the field from 12 o’clock. Scale bar 10  $\mu\text{m}$ . (B)  
852 Average current amplitudes normalized to maximum current for cells expressing ANO6 (red square) or  
853 ANO1 (black circles) plotted vs. time after establishing whole-cell recording. (C) Average Annexin-V  
854 fluorescence normalized to maximum fluorescence for the same cells as in B (n=6).

856 **Figure 4.** Activation of ANO6 current and PLS requires high intracellular  $\text{Ca}^{2+}$  concentrations. (A).  
857 Average current-voltage relationships of currents recorded ~20 min after establishing whole-cell  
858 recording in Ano6-expressing cells patched with 20  $\mu\text{M}$  (black squares, N = 6) or 200  $\mu\text{M}$   $\text{Ca}^{2+}$  (red

859 circles, N = 10) in the patch pipet. **(B)** Annexin-V binding in Ano6-expressing cells patched with 20  $\mu$ M  
860 (black squares, N= 5) and 200  $\mu$ M (red circles, N = 15)  $\text{Ca}^{2+}$  in the patch pipet. Error bars are S.E.M.

861

862 **Figure 5.** Ionic selectivity of ANO6 currents. Representative whole-cell patch-clamp recordings and  
863 current-voltage relationships from **(A)** ANO6 and **(B)** ANO1 expressing cells with 200 $\mu$ M  $[\text{Ca}^{2+}]_i$ .  
864 Currents were recorded in 150 mM or 15 mM extracellular CsCl. The reversal potentials ( $E_{\text{rev}}$ ) shift very  
865 little with ANO6-expressing cells, while the shift is large for ANO1-expressing cells. **(C)** Average  $E_{\text{rev}}$   
866 values for ANO6 or ANO1 expressing cells bathed in 146 NaCl, 150 CsCl, 15 NaCl, 15 CsCl, or 150  
867 NMDG-Cl. **(D)** Relative permeabilities calculated from the Goldman-Hodgkin-Katz equation. N=6-17.

868

869 **Figure 6.** Identification of a PLS domain in ANO6. **(A).** Site-specific Type II divergence scores were  
870 calculated by comparing ANO1 and ANO6 sequences from 24 mammalian species, binned over a 15-  
871 amino acid window, and normalized to the maximum value. Horizontal lines at top indicate  
872 transmembrane domains. Vertical lines indicate individual amino acids with high Type II Divergence  
873 Scores. **(B).** Summary of 1-6-1 chimeras. Black line represents ANO1 sequence with TMDs 2 -10 labeled.  
874 Colored horizontal lines represent ANO1 sequence that was replaced with the corresponding ANO6  
875 sequence. Numbers refer to ANO1 sequence. Green: ANO1-like currents, no scrambling. Red:  
876 scrambling. Grey: weak plasma membrane expression, but no currents or scrambling. Orange: some  
877 plasma membrane expression, no currents or scrambling. **(C).** Scrambling domain. The sequences of  
878 ANO1 (535-601) and ANO6 (506-572) are aligned with TMD 4 and TMD5 indicated. Amino acids are  
879 colored according to Rasmol. Scrambling domain (SCRD) shows region associated with PLS. Asterisks  
880 show amino acids that are essential for PLS in ANO6. Figure supplement 1 lists sequence accession  
881 numbers used for Diverge analysis. Figure supplement 2 shows alignment of mANO1 and mANO6 used  
882 for chimeric construction. Figure supplement 3 tabulates the properties of all of the 1-6-1 chimeras.  
883 Figure supplement 4 shows a confocal image of scrambling by the 1-6-1\_(554-588) chimera. Figure  
884 supplement 5 summarizes properties of mutations in ANO6 SCR D.

885

886 **Figure 6-figure supplement 1.** Genbank accession numbers of sequences of mammalian species ANO1  
887 and ANO6 used for DIVERGE analysis.

888

889 **Figure 6-figure supplement 2.** MUSCLE alignment (McWilliam et al., 2013) of mANO1(ac) and  
890 mANO6 used for constructing chimeras. Blue lines indicate membrane helices 1 – 10 determined by a  
891 homology model based on nhTMEM16 (Brunner et al., 2014).

892

893 **Figure 6-figure supplement 3.** Properties of 1-6-1 chimeras that trafficked to the plasma membrane and  
894 generated ionic currents. Cells were transiently transfected with the indicated constructs in which the  
895 indicated amino acids of mANO1(ac) were replaced with the corresponding amino acids of mANO6 (as  
896 determined by the alignment shown in Figure 5-figure supplement 2). Currents were measured with 20  
897  $\mu$ M free  $\text{Ca}^{2+}$  in the patch pipet at +100 mV or with zero  $\text{Ca}^{2+}$  in the patch pipet at +200 mV. PLS was  
898 measured by Annexin-V-Alexa568 binding to cultures of cells 10 min after addition of 10  $\mu$ M A23187  
899 and 1  $\mu$ M thapsigargin. PLS was assessed in >3 independent experiments, counting >100 cells.

900

901

902 **Figure 6-figure supplement 4.** Properties of 1-6-1 chimeras in which pairs or triplets of amino acids  
903 were mutated. None of these chimeras exhibited PLS.

904

905 **Figure 6-figure supplement 5.** Properties of ANO6 with mutations in the scrambling domain. Various  
906 mutations in the scrambling domain abolish PLS and ionic currents.

907

908 **Figure 7.** Properties of chimeras of ANO1 and ANO6. **(A,B)** Patch clamp analysis of PLS **(A)** and ionic  
909 currents **(B)** in ANO1-ANO6 chimeras. Cells were patch clamped with 200  $\mu\text{M}$   $\text{Ca}^{2+}$  in the pipet and PLS  
910 was monitored by Annexin-V binding and currents measured by voltage steps from 0 mV to +100 mV.  
911 **(C)** Confocal imaging of Annexin-V binding to HEK cells transfected with the 1-6-1\_D554-K588 or the  
912 6-1-6\_N525-I527 chimeras 10 min after elevating  $\text{Ca}^{2+}$  with A23187. **(D.)** Number of cells binding  
913 Annexin-V (“scrambled”) or not binding Annexin-V (“not scrambled”) 10 min after elevation of  $\text{Ca}^{2+}$   
914 with A23187 (N=3 experiments each). **(E.)** Time course of Annexin-V binding to cells expressing the 1-  
915 6-1\_D554-K588 chimera (red) compared to the time course of Annexin binding to ANO1-expressing cells  
916 (black).

917

918 **Figure 7-figure supplement 1.** Patch clamp analysis of ANO1-ANO6 chimeras. HEK cells expressing  
919 **(A)** 1-6-1\_D554-K588 or **(B)** 6-1-6\_N525-I527 were patch clamped in the presence of Annexin-V-Alexa-  
920 568 in the bath. The first image shows ANO6-EGFP fluorescence obtained before establishing whole-cell  
921 recording.  $F_o$  was determined immediately after establishing whole-cell recording. Annexin-V  
922 fluorescence images were acquired immediately after obtaining each I-V curve by voltage clamp at one  
923 minute intervals. The patch pipet contained 20  $\mu\text{M}$  free  $\text{Ca}^{2+}$  for 1-6-1\_D554-K588 and 200  $\mu\text{M}$  for 6-1-  
924 6\_N525-I527. I-V curves were obtained by voltage steps from -100mV to +100 mV in 20 mV increments.  
925 Scale bars 10  $\mu\text{m}$ . **(C)** Average current amplitudes  $\pm$  SEM at +100 mV for 1-6-1\_D554-K588 (red circles)  
926 and 6-1-6\_N525-I527 (black squares) plotted vs. time after establishing whole-cell recording. The red  
927 curve was drawn by hand as the sum of an exponential and a Gaussian with the dashed portion of the  
928 curve representing the exponential curve in the absence of the Gaussian component. **(D)** Average  
929 Annexin-V fluorescence divided by the initial fluorescence  $\pm$  SEM for the same cells as in C (n=5).

930

931 **Figure 8.** Ion channel properties of ANO1-ANO6 chimeras. **(A).** Inhibition of currents by MONNA.  
932 ANO1 is nearly completely blocked by 10  $\mu\text{M}$  MONNA, while ANO6 and the 1-6-1 chimeras that  
933 scramble are not affected. **(B).** Effects of MONNA on currents associated with the 1-6-1\_D554-K588  
934 chimera. MONNA blocks the  $\text{Ca}^{2+}$ -independent current elicited by depolarization to +100mV (blue  
935 triangles), but has no effect on the  $\text{Ca}^{2+}$ -activated current after scrambling has occurred (red squares). In  
936 contrast, before scrambling has occurred, MONNA partially blocks the  $\text{Ca}^{2+}$ -activated current (open  
937 circles). **(C-F).** The ionic selectivity of currents associated with the 1-6-1\_D554-K588 chimera **(C-D)** and  
938 the 1-6-1\_S532-G558 chimera **(E-F)** were determined by the dilution method (see Methods) by  
939 measuring reversal potentials with external solutions containing either 150 mM (black line) or 15 mM  
940 (red line) CsCl. **(C)**  $\text{Ca}^{2+}$ -independent (zero  $\text{Ca}^{2+}_i$ ) and **(D)**  $\text{Ca}^{2+}$ -activated currents associated with the 1-  
941 6-1\_S532-G558 chimera. Currents recorded **(E)** before and **(F)** after scrambling with the 1-6-1\_S532-  
942 G558 chimera. N=3-7. Error bar represents SEM.

943 **Figure 9.** Homology model of ANO6. **(A).** Side view from the membrane. ANO6 is shown as a dimer  
944 with the left subunit in gold and the right subunit in grey. The scrambling domain (SCRD) is colored red.  
945 Transmembrane helices are numbered. **(B).** View from extracellular side. **(C)** View from cytoplasm. **(D)**  
946 A view from the membrane looking towards the hydrophilic cleft showing the SCRD in red and the  $\text{Ca}^{2+}$   
947 binding site in stick representation. Residues conserved between ANO6 and TMEM16 that coordinate  
948  $\text{Ca}^{2+}$  (green) are shown as white sticks (C=white, O=red). ANO6 contains GXXX (pink), which is a D503  
949 in TMEM16. **(E).** Close-up view of D. **(F)** Same view as D with surface colored to show hydrophilicity.  
950 Green: hydrophilic. White: hydrophobic.

951

952 **Figure 9-figure supplement 1.** Homology model of ANO1 dimer. The SCRD homology domain is  
953 colored red. The  $\text{Ca}^{2+}$  binding site is shown in stick representation in the right monomer. Residues  
954 identified by Yu et al. (2012) as forming the vestibule of the ion conduction pathway of ANO1 are shown  
955 in spacefill (C625, G628-M632, I636-Q637).

956

957

958 **Figure Supplements.**

959

960 **Figure 6-figure supplement 1.** Genbank accession numbers of sequences of mammalian species ANO1  
961 and ANO6 used for DIVERGE analysis.

962 **Figure 6-figure supplement 2.** MUSCLE alignment (McWilliam et al., 2013) of mANO1(ac) and  
963 mANO6 used for constructing chimeras.

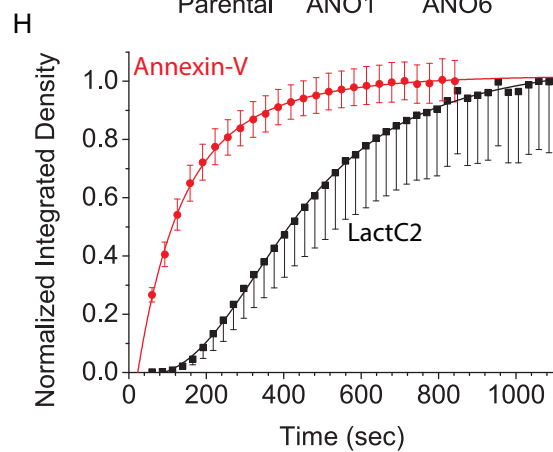
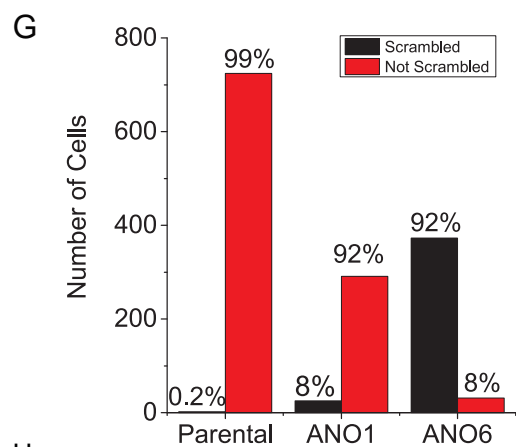
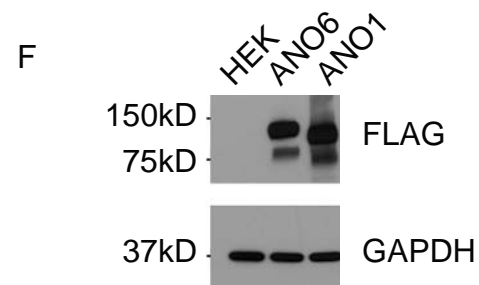
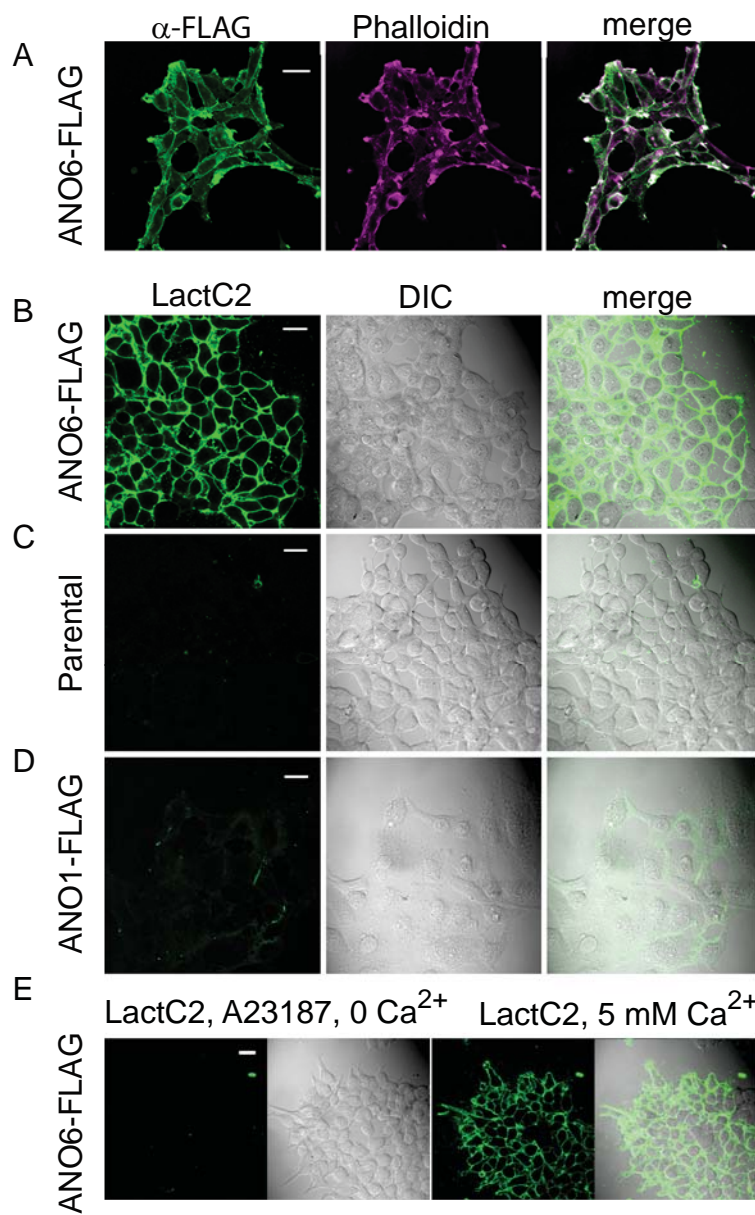
964 **Figure 6-figure supplement 3.** Properties of 1-6-1 chimeras that trafficked to the plasma membrane and  
965 generated ionic currents.

966 **Figure 6-figure supplement 4.** Properties of 1-6-1 chimeras in which pairs or triplets of amino acids  
967 were mutated. None of these chimeras exhibited PLS.

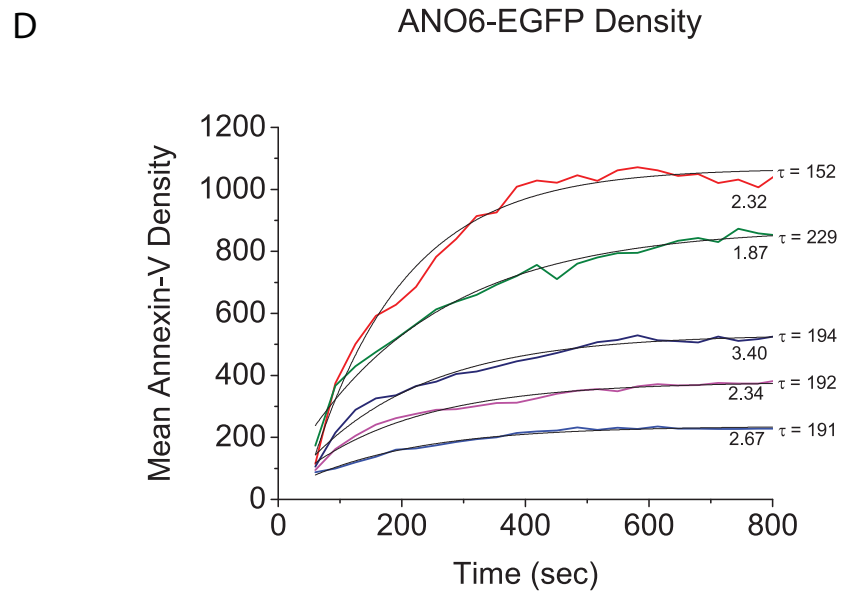
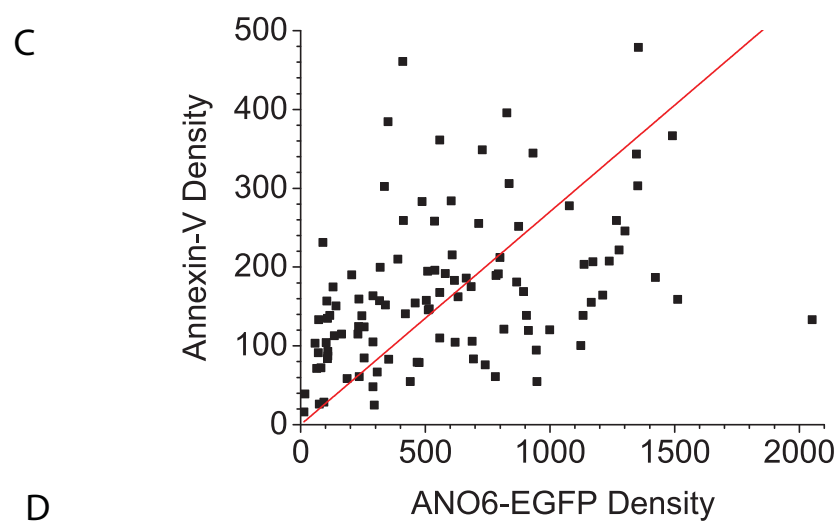
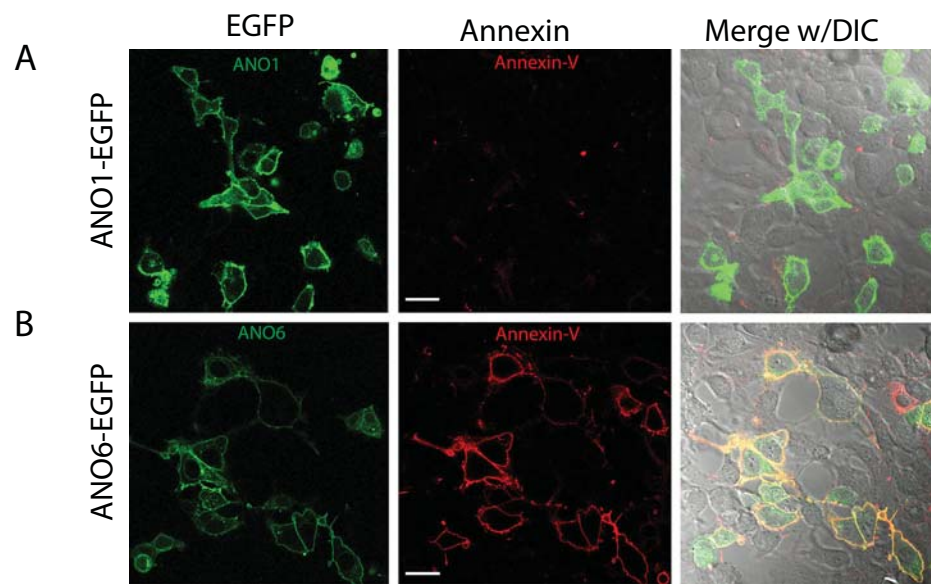
968 **Figure 6-figure supplement 5.** Properties of ANO6 with mutations in the scrambling domain. Various  
969 mutations in the scrambling domain abolish PLS and ionic currents.

970 **Figure 7-figure supplement 1.** Patch clamp analysis of ANO1-ANO6 chimeras.

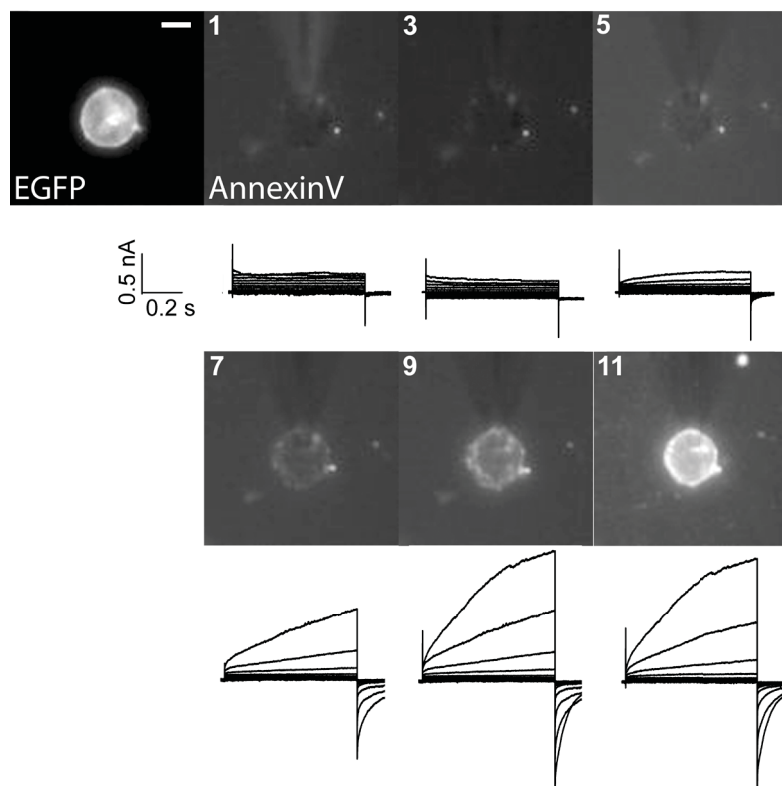
971 **Figure 9-figure supplement 1.** Homology model of ANO1 dimer.



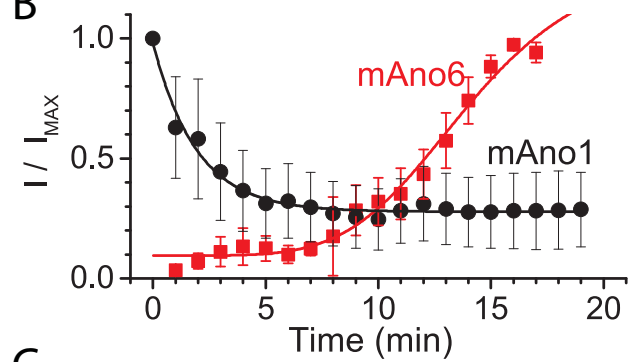




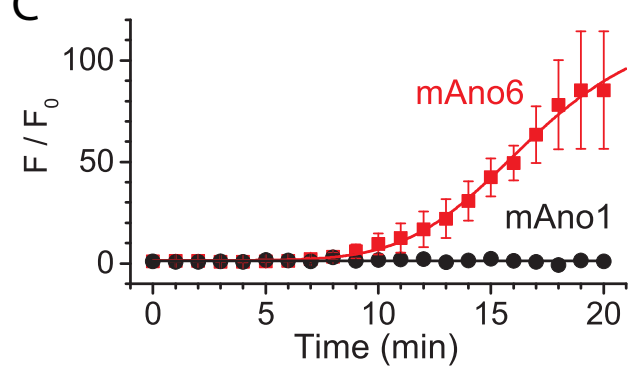
A

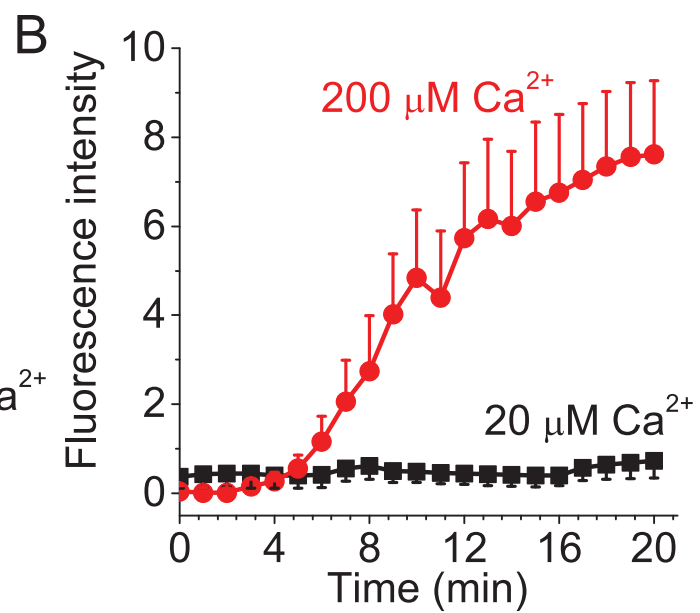
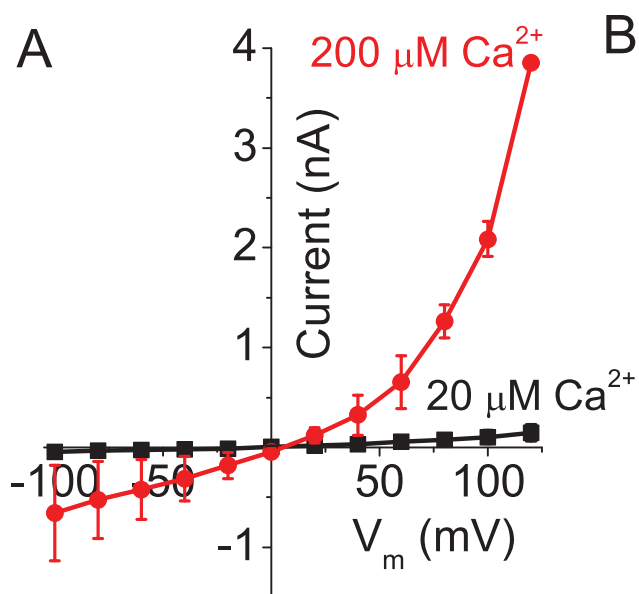


B

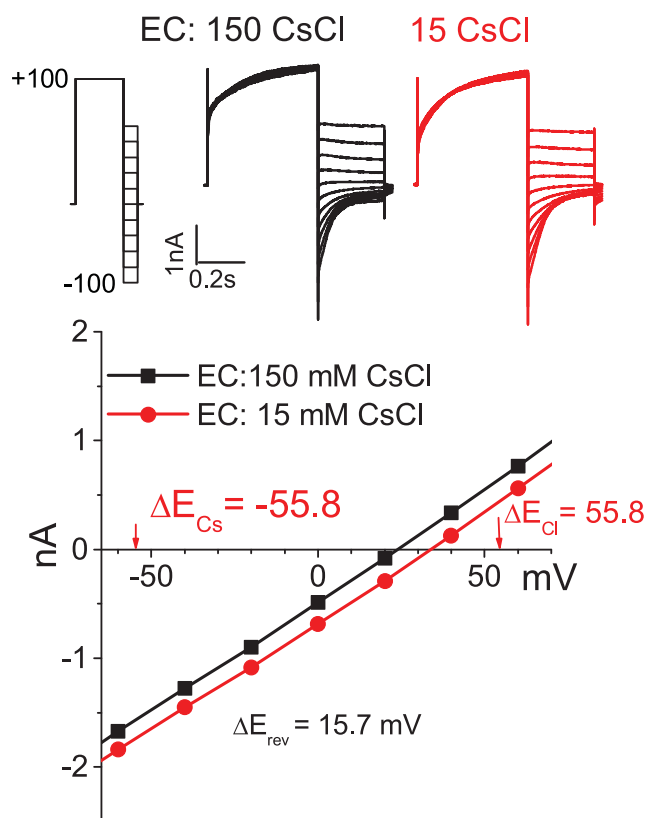


C

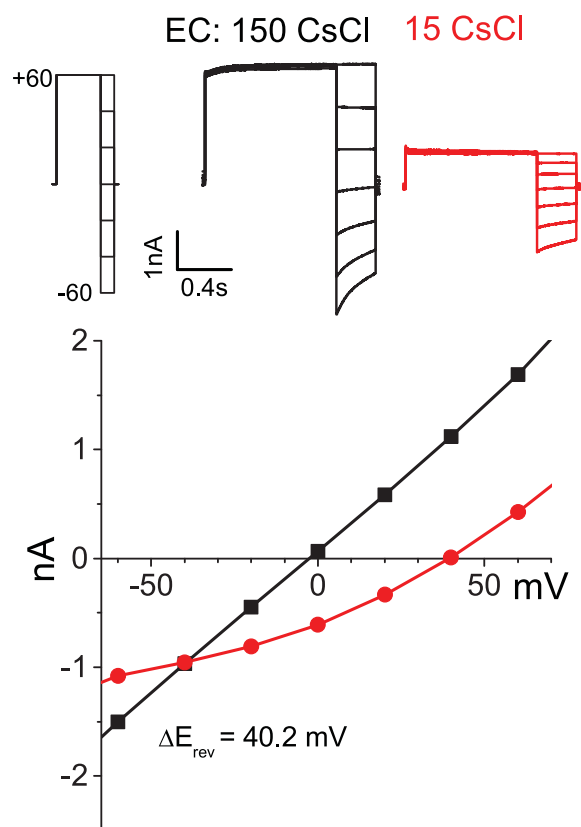




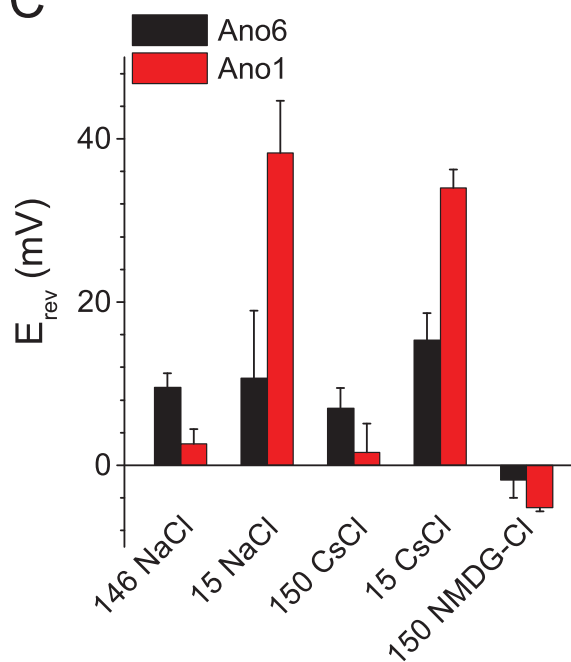
## A. ANO6



## B. ANO1



## C



## D

